Performance of a Boundary Layer Ingesting Propulsion System

by

Angélique Plas

Diplôme de l'Ecole Polytechnique (2006)

Submitted to the Department of Aeronautics and Astronautics
in partial fulfillment of the requirements for the degree of

Master of Science in Aeronautics and Astronautics

at the

MASSACHUSETTS INSTITUTE OF TECHNOLOGY

June 2006

Author .....
Department of Aeronautics and Astronautics
May 26, 2006

Certified by. .....
Edward Greitzer
H.N. Slater Professor in Aeronautics and Astronautics
Thesis Supervisor

Accepted by .....
Jaime Peraire
Chair, Committee on Graduate Students

Performance of a Boundary Layer Ingesting Propulsion System

by

Angélique Plas

Submitted to the Department of Aeronautics and Astronautics
on May 26, 2006, in partial fulfillment of the
requirements for the degree of
Master of Science in Aeronautics and Astronautics

Abstract

This thesis presents an assessment of the aerodynamic performance of an aircraft propulsion system, with embedded engines, in the presence of aircraft fuselage boundary layer ingestion (BLI). The emphasis is on defining the role that the turbomachinery (i.e., the fan, in the ultra high bypass engines considered) plays in establishing the flow benefit due to BLI. A three-dimensional body force approach to fan response to inlet distortion has been utilized to analyze the flow in the engine ducts. In addition to providing quantitative information as to the fuel burn benefit from BLI, the body force approach is also compared with two simpler analyses, one based on the parallel compressor concept and one based on integral boundary layer methodology.

It is shown that the distortion transfer across the fan, basically attenuation of the stagnation pressure non-uniformity downstream of the fan compared to that upstream of the fan plays a major role in determining the impact of boundary layer ingestion on fuel burn. This, in turn, puts requirements on the fidelity with which one needs to assess the distortion transfer, and thus the type of models to be used in such assessment. In terms of qualitative information, the three models are found to give broadly similar trends for distortion attenuation and for fuel burn benefit. In terms of quantitative results, the body force analysis shows that for a fan diameter and flight condition representative of that employed in the Cambridge-MIT Institute "Silent Aircraft" boundary layer ingestion can provide decreases in fuel burn of up to 3.8 percent.

Thesis Supervisor: Edward Greitzer
Title: H.N. Slater Professor in Aeronautics and Astronautics

Acknowledgments

My first thanks go to my thesis supervisor Professor Greitzer. I want to express my deep gratitude to him for his guidance, invaluable advice, and constant encouragement in this challenging research. I would also like to thank him for his excellent and innovative teaching methods, which radically changed my view of engineering, research and engine design.

I am also indebted to Professor Drela for sharing with me his expert knowledge on boundary layers, and for providing always useful comments and suggestions. I want to thank Dr. Gong for helping me with his 3-D code, and Dr. Hynes from Cambridge University for his very useful insights into my research topic.

I gratefully acknowledge the Cambridge-MIT Institute which funded this work, and all the members of the Silent Aircraft Initiative — especially Professor Spakovszky for his constant enthusiasm, Matthew Sargent for the inspiring discussions about thrust and drag with BLI, Vahid Madani for his inlet calculations and fast email replies, Dan Crichton for his fan design, and Dr. Hall and Dr. de la Rosa Blanco for their help. To my officemates, thank you for your support, your good mood, for teaching me the American spirit and for the great time we had during these two years even when working.

Without the French team those two years would not have been the same. Many thanks to all of them for their refreshing "Frenchness" and the ritual lunch at the Whitehead dining room. We surely contributed to keep the place busy.

Finally, I would like to thank my parents, Christian and Pascale Plas, my brother Antoine, and my sister Amandine, for their love, their encouragement, and their support throughout my life. I would not have made it to MIT without them and the priceless education that they gave me. Last but not least, I want to thank somebody

really special to me, who was my greatest support at MIT, my love, Serge Tournier.

Contents

List of Figures

List of Tables

Nomenclature

Roman symbols

b	span of ingested boundary layer, m
c_p	specific heat capacity par unit mass at constant pressure, $J \cdot kg^{-1} \cdot K^{-1}$
h	enthalpy, $kg\ m^2 \cdot s^{-3}$
k	recovery of the boundary layer across the fan, *non-dimensional*
$\dot{m}$	mass flow, $kg \cdot s^{-1}$
p	pressure, Pa
s	entropy per unit mass, $J \cdot kg^{-1} \cdot K^{-1}$
t	slope of the fan characteristic, *non-dimensional*
u	velocity, $m \cdot s^{-1}$
x, y	cartesian coordinates, m
A	area or area per unit depth, m^2 or m
B	blockage factor, *non-dimensional*
C_D	dissipation coefficient, drag coefficient, *non-dimensional*
C_f	skin friction coefficient, *non-dimensional*
C_L	lift coefficient, *non-dimensional*
D	drag, N
E	energy, J
F	propulsive force, N
H	shape factor, *non-dimensional*
H^*	energy factor, *non-dimensional*
H^{**}	density factor, *non-dimensional*

H_k	kinetic shape factor, *non-dimensional*
L	length, m
L/D	lift to drag ratio, *non-dimensional*
KE	kinetic energy given to the flow, J
M	mach number
P	fan power, $J \cdot s^{-1}$
PSC	power saving coefficient, *non-dimensional*
R	wake recovery or universal gas constant, *non-dimensional* or $J \cdot kg^{-1} \cdot K^{-1}$
Re_θ	momentum thickness Reynolds number, *non-dimensional*
$\dot{S}$	rate of entropy, $J \cdot K^{-2} \cdot s^{-1}$
T	thrust or temperature, N or K
U	fan blade tip speed, $m \cdot s^{-1}$
U_s	effective wall slip velocity, $m \cdot s^{-1}$
V	velocity, $m \cdot s^{-1}$
W	duct width, m

Greek symbols

α_3	fluid outlet angle from the stator, *rad*
β_2	fluid outlet angle from the rotor, *rad*
δ	boundary layer thickness, m
δ^*	boundary layer displacement thickness, m
δ^{**}	boundary layer density thickness, m
η	efficiency, *non-dimensional*
η_c	Brayton cycle efficiency, *non-dimensional*
η_{KE}	efficiency for converting shaft power into kinetic power, *non-dimensional*
γ	specific heat ratio, *non-dimensional*
μ	dynamic viscosity, $Pa \cdot s^{-1}$
ϕ	flow coefficient, *non-dimensional*

ψ	stage loading factor, *non-dimensional*
ρ	density, kg/m^3
θ	boundary layer momentum thickness, m
θ^*	boundary layer pseudo-energy thickness, m
τ	temperature ratio or shear stress, *non-dimensional* or Pa
τ_w	wall shear stress, Pa
Π	pressure recovery, *non-dimensional*

Subscripts

0	at station 0 (upstream of the engine), for a velocity V: flight speed, for a length: relative to the precompression region
1	relative to the inlet
2	relative to the exhaust
∞	at station ∞ (freestream)
avg	average
d	downstream of the fan
e	at station e (exit of the engine)
f	at station f (fan / actuator disk), relative to the fan, relative to fuel
i	at station i (inlet)
j	at station j (jet, Trefftz Plane)
jw	relative to the wake at station j
p	propulsive
ref	reference
t	stagnation
th	thermal
u	upstream of the fan
w	relative to the wake that is ingested
A	airframe

B	blocked
E	at the edge of the boundary layer
N	net

Subsubscripts

1	relative to the freestream (high speed flow)
2	relative to the boundary layer (low speed flow)

Superscripts

*	without boundary layer ingestion
$^-$	average
$^{-M}$	mass average

Abbreviations

BLI	Boundary Layer Ingestion
BPR	Bypass Ratio
BWB	Blended Wing Body
CFD	Computational Fluid Dynamics
CMI	Cambridge - MIT Institute
IBLE	Integral Boundary Layers Equations
MIT	Massachusetts Institute of Technology
NASA	National Aeronautics and Space Administration
SAI	Silent Aircraft Initiative
SFC	Specific Fuel Consumption

Chapter 1

Introduction

1.1 Boundary Layer Ingestion

Boundary layer ingestion (BLI) in the context used here means taking fuselage boundary layer fluid through the engine for the purposes of improving fuel efficiency. Boundary layer ingestion occurs in ships and torpedoes and provides this attribute. It has been investigated for aircraft, especially by Boeing with the Blended Wing Body (BWB) program. This thesis presents an assessment of BLI in the conceptual design of the Cambridge - MIT Institute (CMI) "Silent Aircraft" which has the goal of reducing the aircraft noise below the ambient noise of a well-populated area. This thesis includes a rigorous treatment of the non-uniform flow through the engine; estimating the distortion transfer across the fan is a critical item in the assessment.

The benefit of boundary layer ingestion comes from re-energizing the aircraft wake, allowing lower energy waste. This is illustrated using the two idealized situations in Figure 1-1: no boundary layer ingestion (podded engines) and ideal boundary layer ingestion (100% of the wake ingested by the engine). With podded engines the flow entering the engine is at freestream velocity u_∞. The engine accelerates the flow to a velocity u_j, such that the created momentum excess balances the momentum deficit

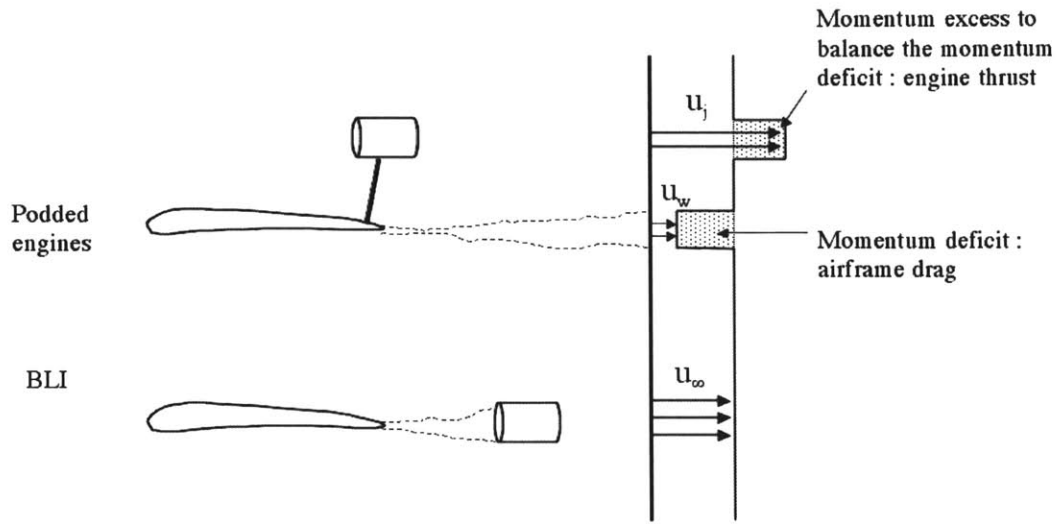

Figure 1-1: Benefits of BLI: podded case and 100% BLI.
The momentum excess created by the podded engine is equal to the momentum deficit of the airframe.

due to the drag of the airframe D_A.

$$F_{engine} = \dot{m}(u_j - u_\infty) = \dot{m}(u_\infty - u_w) = D_A. \tag{1.1}$$

The rate of mechanical energy, $P_{added,\ no\ BLI}$, given to the flow by the engine is:

$$P_{added,\ no\ BLI} = \frac{\dot{m}}{2}\left(u_j^2 - u_\infty^2\right) = \frac{F}{2}\left(u_j + u_\infty\right). \tag{1.2}$$

The power required for flight (the useful power) is:

$$P_{useful} = D_A u_\infty = \dot{m}\left(u_j - u_\infty\right) u_\infty. \tag{1.3}$$

Suppose all the boundary layer is ingested and the engine accelerates the wake back to freestream. The force provided by the engine is:

$$F_{engine} = \dot{m}(u_j - u_w) = \dot{m}(u_\infty - u_w) = D_A. \tag{1.4}$$

The rate of energy given to the flow by the engine, $P_{added,\ BLI}$, is:

$$P_{added,\ BLI} = \frac{\dot{m}}{2}\left(u_j^2 - u_w^2\right) = \frac{\dot{m}}{2}\left(u_\infty^2 - u_w^2\right) = \frac{F}{2}\left(u_w + u_\infty\right). \tag{1.5}$$

The power required for flight is the same as with podded engines:

$$P_{useful} = D_A u_\infty = \dot{m}\left(u_j - u_w\right) u_\infty. \tag{1.6}$$

Since $u_j > u_w$, comparison of equations (1.2) and (1.5) shows,

$$P_{added,\ no\ BLI} > P_{added,\ BLI}. \tag{1.7}$$

Less power is required to sustain the same drag force on the airframe with boundary layer ingestion.

The difference in energy input between the two situations occurs because, for a specific force, less power needs to be added to a flow that enters the engine with a lower velocity. Consider a flow that enters an engine at velocity u_1 and exits at velocity u_2. The force created by the engine is:

$$F = \dot{m}\left(u_2 - u_1\right) = \dot{m}\Delta u. \tag{1.8}$$

The power put into the flow is:

$$P = \frac{\dot{m}}{2}\left(u_2^2 - u_1^2\right) = F\frac{u_1 + u_2}{2} = F\left(u_1 + \frac{\Delta u}{2}\right). \tag{1.9}$$

For constant mass flow and constant propulsive force, Δu is constant. A decrease in u_1 results in a decrease in power. In other words for lower inlet velocity, i.e. for the case of ingesting boundary layer fluid, the same propulsive force can be achieved with less power[1].

[1]An analogous result can be derived for constant engine diameter and constant propulsive force

1.2 Embedded engines vs. podded engines

BLI cannot be achieved with podded engines which are out of the fuselage boundary layer. It requires embedded engines which are partly buried in the airframe. A blended-wing-body (BWB) type aircraft, with embedded engines that ingest part of the boundary layer from the fuselage upper surface, is the configuration used in the CMI Silent Aircraft Initiative (SAI).

In the SAI design, the engines are embedded in the aft upper part of the fuselage because of balance requirements[2]. The installation offers the opportunity to swallow a substantial part of the centerbody boundary layer (15% of the bare airframe drag) and allows for a reduction in wetted area and structural weight because of the disappearance of pylons. In addition the embedded engines produce a thrust line closer to the centerline, reducing nose-down pitching moment arising with podded engines. This diminishes "trim problems along with control surface size and power requirements" (Campbell et. al. [2]). In terms of noise, embedding provides the ability to package high bypass ratio engines and liners in the exhaust duct to reduce noise (Sargent [32]) and shields the engine noise perceived by people on the ground.

Embedding the engines, however, introduces several possible drawbacks. First the airframe and engine designs become much more coupled. Second, ingesting boundary layer results in a non-uniform flow in the inlet and at the fan face which may result in operability issues and a decreased performance of the engine. This non-uniformity is exacerbated by the curvature of the duct[3]. The resulting pressure gradients produce secondary flows and may lead to boundary layer separation. According to Rodriguez [31], "Inlet flow separation becomes a distinct possibility since the inlet must diffuse (via an adverse pressure gradient) an already well-developed boundary layer". Distortion at the fan face may produce additional vibration and noise (Dowling, Hynes [10]). Distortion may also "cause structural and operational difficulties with the en-

[2]Embedding them under the fuselage would also require very large landing gears and cause difficulties with runway clearances (Liebeck [26])

[3]The curvature is necessary because the flow must be turned so as to follow the airfoil curvature at the exhaust. Besides, the duct has to be curved to gain wetted area (Sargent [32])

Table 1.1: Advantages and drawbacks of different propulsion systems

	Podded engines	Embedded engines with BLI
Advantages	• Proven technology • Captures uniform flow	• BLI → Fuel burn benefits • Liners and high BPR fans can be packaged more easily → Noise benefits • Nacelle wetted area savings • Weight savings • Lower thrust line
Drawbacks	• Larger wetted area • Larger structural weight (pylons and nacelles) • Pylon-airframe interference • High thrust line gives nose-down pitching moment	• Non-uniform flow and S-duct → Possible degradation of inlet performance (separation, secondary flows) • Distortion at the fan face → vibration, noise? • Operability issues • More integrated design necessary • Unproven technology

gine as well as deteriorate performance" (Lynch, [29]). Last but not least, podded engines are a proven technology, whereas embedded engines are a new configuration that involves risk. Table 1.1 summarizes the advantages and drawbacks of embedding the engines.

1.3 Objectives

The objective of this thesis is the examination of the impact of ingesting boundary layer on the fuel burn of a high bypass ratio engine, comparing the performance of a boundary layer ingesting propulsion system to that of a podded system. The principal success criteria is obtaining quantitative assessment of the performance of both systems using models of an appropriate level of fidelity. This level will be defined later in the thesis.

1.4 Scope of research and thesis overview

The next chapter reviews the available literature, discusses the major issues in dealing with BLI, explains the approach taken to address them, and gives the rationale behind the level of models used in this thesis. Chapter 3 describes the results of a simple approach based on a 1-D parallel compressor model and analyzes the obtained results. Chapter 4 discusses integral, boundary layer-like, models. The last chapter discusses 3-D fan distortion transfer calculations and provides evaluation of both the impact on power and the relative capability of the different models.

1.5 Contributions

The contributions of this thesis are:

1. Creation of a conceptual and theoretical framework for modeling boundary layer ingestion in aircraft design including definition of the key issues in aircraft performance with BLI;

2. Development of high fidelity models for representing an aircraft with boundary layer ingesting embedded engines;

3. Quantification of the benefits of BLI.

Chapter 2

Research focus

2.1 Previous studies

Studies on BLI have focused mainly on the effect of a wake on propeller performance. Smith [35] carried out the first study on boundary layer ingestion that the author has found. He examined an engine that inducts boundary layer air and showed that a 5 to 10% reduction in cruising fuel consumption was achievable. He also discussed the design, operability and performance of an aircraft with engines that induct boundary layer air to reduce the "skin friction drag by proper control of the boundary layer". The concept was to remove boundary layer by suction through slots in the wing and the fuselage to delay transition of the laminar boundary layer. Smith discusses the issues associated with the design of slots and ducts that assure the stability of the boundary layer, the stability and control characteristics of such a configuration, and the impact of boundary layer ingestion on maximum lift. He then compares three configurations: a turboprop engine, a turbojet engine, and a turbojet engine with boundary layer suction. His main results, based on test data (component tests and German propeller-driven aircraft tests), showed the engines he investigated with boundary layer suction had better control characteristics, reduced runway length requirements, increased C_L and L/D, increased maximum speed, and reduced fuel consumption by 32% compared to a turbojet engine propelling the same airframe.

Lynch [29] carried out a performance analysis of a boundary layer ingesting turbofan. He assumed no change in airframe drag with boundary layer ingestion, and a one-seventh power boundary layer profile. He also assumed that the boundary layer is completely mixed at the fan face, and that the net drag is equal to the bare airframe drag minus the momentum defect of the ingested boundary layer. Results were obtained for two different values of inlet losses. There was a 3% reduction in SFC for the lowest value of inlet losses, no savings for the largest one, and a 6-10% reduction in maximum effective thrust if only the gas generator ingests boundary layer air.

Betz [1] analyzed a propeller in a wake which ingests all the airframe drag at ambient static pressure. He showed that the required power is reduced because there is no energy excess left in the slipstream from the propeller and the engine uses the energy that is left in the wake.

Douglass [9] carried out a study of an aircraft with BLI. The engine characteristics and V_e/V_0 were kept the same as for the non-ingesting case (V_e is the velocity increment given by the engine to the flow and V_0 is the flight speed). Compressibility was neglected, a one-seventh power profile was used for the ingested boundary layer, and the flow was assumed to enter the engine at ambient static pressure. He found that boundary layer ingestion is beneficial because it means a reduction in the kinetic energy of both the wake and the jet. Douglass calculated a maximum improvement in propulsive efficiency of 28% for torpedoes and 16% for a typical airplane, provided there are no losses in the inlet. Douglass also assessed the impact of BLI on the Brayton cycle efficiency η_C for a turbojet or turbofan gas generator. η_C depends on the overall compression ratio, compression efficiency, turbine efficiency, temperature ratio and specific heat ratio. BLI impacts the cycle efficiency by modifying the overall compression ratio and efficiency. Douglass showed that η_C is reduced by 6.1% to 21% with inlet losses and BLI. The overall efficiency can thus be reduced or improved with boundary layer ingestion.

Smith [36] carried out a detailed analysis of an axisymmetric unducted propeller ingesting a wake using an actuator disk. The conditions were incompressible flow, no viscous forces or mixing, ambient static pressure at the inlet (in other words, the body and the propeller are decoupled: the propeller is far behind the body), and the wake keeps its profile across the propeller.

Smith defined a power saving coefficient as the ratio of the difference between the propulsive powers without BLI, and with BLI, to the power necessary to propell the part of the body whose drag is to be ingested, evaluated for no BLI. The comparison was done at constant propulsor diameter and constant η_{KE} "which is the efficiency for converting shaft power into jet axial kinetic energy flux", or propulsive power. He found that the power saving coefficient is a function of the ratio of boundary layer displacement thickness to boundary layer thickness δ^*/δ, the shape factor H, the energy factor H^*, the wake recovery R defined as

$$R = 1 - \frac{V_j - V_{j_w}}{V_0 - V_w}, \tag{2.1}$$

(where V_0 is the flight velocity, V_w the ingested wake veloctity, V_j the jet velocity, and V_{j_w} the jet velocity in the wake), the airframe drag coefficient C_{D_A}, and the ratio of ingested drag to airframe drag D_w/D_A. His main results are that benefits can be up to 7% if all the wake is ingested ("wake ingestion ideal case"), that the power savings are not very sensitive to the wake recovery; and that the power savings are higher for higher H and are greater for higher thrust loadings.

Rodriguez [31] performed an analysis of unducted and ducted propulsors based on actuator disk assumptions (Küchemann and Weber [25]). The flow was assumed incompressible, at ambient static pressure at the inlet (again this means decoupled body and engine), and ideally mixed in front of the actuator disk. The velocity at the actuator disk was assumed to be:

$$u_{f_{duct}} = u_{f_{no\ duct}} + \Delta u, \tag{2.2}$$

where u_f is the fan face mixed out velocity. Rodriguez calculated 2.2% increase in propulsive efficiency for 3.6% ingested drag. The propulsive efficiency was found to be a function of the velocity increment Δu, the ratio of ingested drag to airframe drag D_w/D_A, and the airframe drag coefficient C_{D_A}.

The above summary of the exisiting work on BLI shows that there has been no analysis of the reponse of a fan to BLI and how it affects the performance for a ducted fan. That is the topic of this thesis.

2.2 Research issues

The following questions must be addressed in developing a useful representation of the flow:

- how do we decribe the flow of interest?
- what are the characteristics of the flow to capture?
- what should be compared and how?
- what is an appropriate figure of merit?

The remainder of the chapter will focus on answering these questions.

2.3 Flow description

Features of the Silent Aircraft propulsion system are shown in Figure 2-1. Starting from upstream there is first a "precompression zone" where the flow begins to be modified by the engine. At the start of this region, there is a boundary layer on the fuselage and the conditions are different than upstream infinity. This boundary layer can be characterized by several integral parameters (Drela [11]). The displacement thickness is defined as:

$$\delta^* = \int_0^\delta \left(1 - \frac{\rho u}{\rho_E u_E}\right) \mathrm{d}y, \tag{2.3}$$

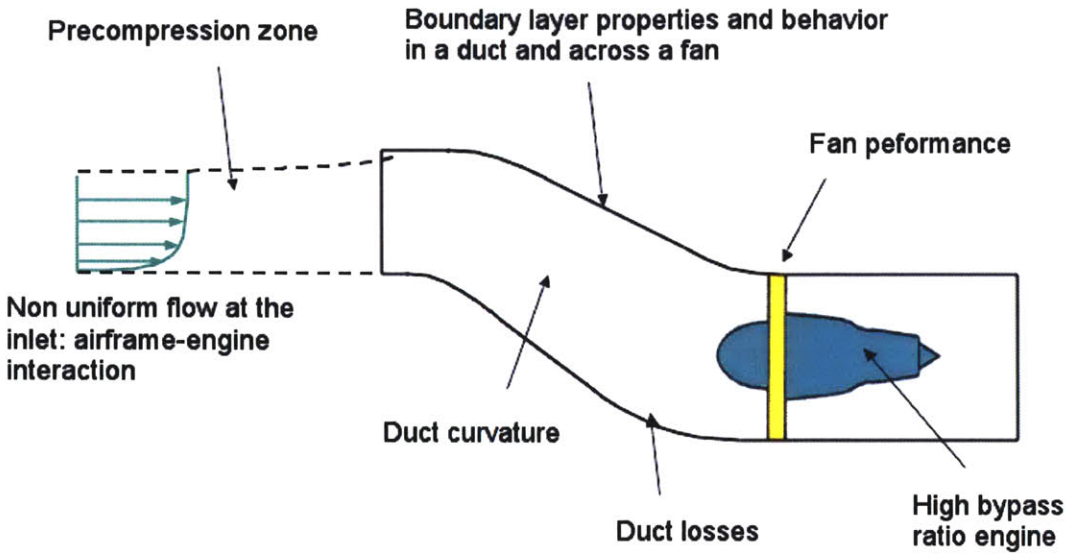

Figure 2-1: Features of the propulsion system of the Silent Aircraft

where u_E and ρ_E are the velocity and density at the edge of the boundary layer, and δ is the boundary layer thickness. This represents the flow blockage. Consider a uniform flow of velocity u_E and density ρ_E passing through a duct of width W. The mass flow is

$$\dot{m}_{\text{uniform}} = \int_0^W \rho u \, \mathrm{d}y = \rho_E u_E W. \tag{2.4}$$

Consider now a viscous flow of the same edge velocity u_E, and density ρ_E, and of boundary layer thickness W. The mass flow is:

$$\dot{m}_{\text{viscous}} = \int_0^W \rho u \, \mathrm{d}y = \rho_E u_E W - \int_0^W (\rho_E u_E - \rho u) \, \mathrm{d}y = \dot{m}_{\text{uniform}} - \rho_E u_E \delta^*. \tag{2.5}$$

The difference between the actual (2.5) and uniform (2.4) mass flows is the mass flow defect $\rho_E u_E \delta^*$ due to the boundary layer.

The momentum thickness is defined as:

$$\theta = \int_0^{\delta} \left(1 - \frac{u}{u_E}\right) \frac{\rho u}{\rho_E u_E} \, \mathrm{d}y. \tag{2.6}$$

$\rho_E u_E^2 \theta$ represents the momentum defect of the viscous flow compared to the same mass flow at uniform velocity. The energy thickness is:

$$\theta^* = \int_0^{\delta} \left(1 - \left(\frac{u}{u_E}\right)^2\right) \frac{\rho u}{\rho_E u_E} \, \mathrm{d}y. \tag{2.7}$$

$\rho_E u_E^3 \theta^*$ represents the energy defect of the viscous flow compared to the same mass flow at uniform velocity. The density thickness is defined as:

$$\delta^{**} = \int_0^{\delta} \left(1 - \frac{\rho}{\rho_E}\right) \frac{u}{u_E} \, \mathrm{d}y. \tag{2.8}$$

$\rho_E u_E \delta^{**}$ represents the mass flow defect of the viscous flow of non-uniform density compared to a viscous flow of uniform density and same velocity profile.

Non-dimensional parameters describing the boundary layer are the shape factor

$$H = \frac{\delta^*}{\theta}, \tag{2.9}$$

the energy factor

$$H^* = \frac{\theta^*}{\theta}, \tag{2.10}$$

the density factor

$$H^{**} = \frac{\delta^{**}}{\theta}, \tag{2.11}$$

and the displacement thickness to boundary layer thickness ratio,

$$\frac{\delta^*}{\delta}. \tag{2.12}$$

In the embedded configuration after the flow enters the inlet, it passes through an "S-duct". Duct losses associated with inlet curvature are being assessed by Madani of Cambridge University [30]. It is assumed here that the duct can be designed well enough (or flow control such as vortex generators can be used) so that separation will not occur and effects of curvature are not considered.

The distortion presented to the fan is a so-called "smile": the bottom part of the fan face flow has lower stagnation pressure. It is thus a combination of circumferential and radial distortion. The fan interacts with the distortion, generally producing a *distortion transfer* across the fan in which the exit stagnation pressure profile is different than the inlet profile, and in which an exit stagnation temperature non-uniformity is typically created.

The bypass ratio (BPR) is large (around 15) for the Silent Aircraft so that most of the power given to the flow comes from the fan. The core flow is thus not described in detail, and the thesis concentrates on a ducted fan representation.

2.4 Features to be captured

The features of the propulsion system that need to be captured are:

- boundary layer and inviscid flow properties at the start and end of the precompression zone, i.e. distribution of the flow entering the inlet
- inlet duct and nozzle behavior with non-uniform flow (straight duct)
- losses: entropy rise in intake, fan and exhaust
- boundary layer properties along the duct
- ducted fan performance (power and efficiency) with distortion
- distortion transfer across the fan

- overall thrust with distortion

A sketch of the ducted fan system showing the different stations is given in Figure 2-2.

- Station ∞: freestream.
- Station 0: the engine does not affect the flow upstream of this station. This is the start of the precompression zone, approximately two inlet diameters upstream of the inlet.
- Station i: inlet lip highlight plane.
- Station f: propulsor / fan. When needed, station u is the inlet of the fan and station d is the exit of the fan.
- Station e: exit of the engine (nozzle).
- Station j: Trefftz Plane where the engine flow is at ambient static pressure. For subsonic flow, stations e and j are the same.

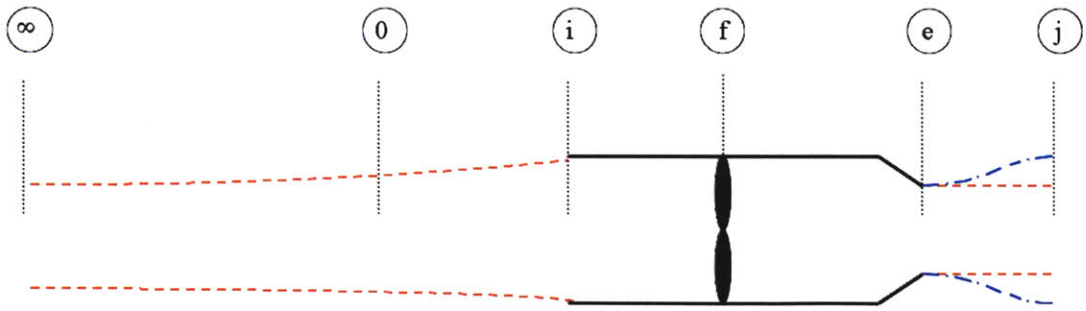

Figure 2-2: Schematic of a ducted fan showing station nomenclature
The red dashed flow between station e and j represents the subsonic case where the exit static pressure is the freestream static pressure. The blue dotted - dashed flow represents the choked or supersonic case where the nozzle is choked and the flow expands to ambient static pressure.

2.5 Control volumes for BLI assessment

In the podded case, the definition of an appropriate control volume for the study of the engines is clear because the engines and airframe are separate. Following Hill and Peterson [21], a control volume can be defined as including the flow that goes through and around the engine from freestream to the "Trefftz Plane", the plane downstream of the aircraft where the flow has returned to freestream static pressure. This control volume is sketched in Figure 2-3. The flow at the upper and lower

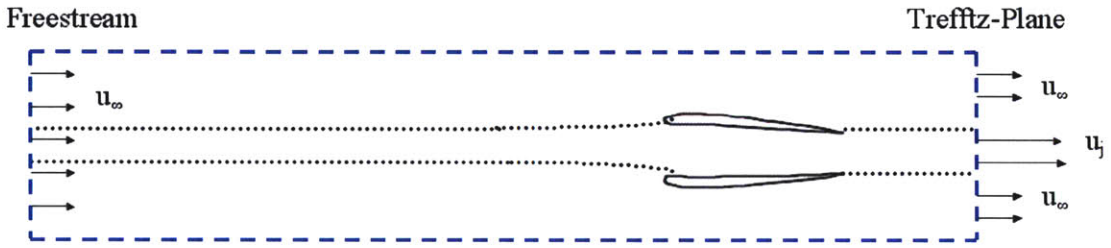

Figure 2-3: Control volume for a podded engine

boundaries of this control volume is considered as being far enough to be undisturbed by the airframe and the engine. The flow that does not go through the engine is at freestream conditions at the boundaries of the control volume and its momentum cancels out of the overall momentum equation. The propulsive force created by the engines is, neglecting the fuel mass flow,

$$T = \dot{m}(u_j - u_\infty), \tag{2.13}$$

where $\dot{m}$ is the engine mass flow and u_j is the jet velocity at the Trefftz Plane[1]. This propulsive force balances the bare airframe drag (if nacelle drag is neglected):

$$D_A = \int \rho(u_\infty - u_w)u_w \, \mathrm{d}A. \tag{2.14}$$

[1]The definition does not include a pressure force for a choked nozzle as in Hill and Peterson [21] because the velocity is estimated at the Trefftz Plane and not at the nozzle exit

For an embedded engine it is not possible to separate the airframe and engine influence on the flow. The force on a control volume including the flow from the start of the precompression zone to the Trefftz Plane, as sketched in Figure 2-4, is not only the engine propulsive force but also the pressure forces that come from the airframe curvature, referred to as the "potential field effect" by Smith [36]. Further, the flow that does not go through the engine is not at freestream conditions at the control volume boundaries and its actual momentum needs to be accounted for.

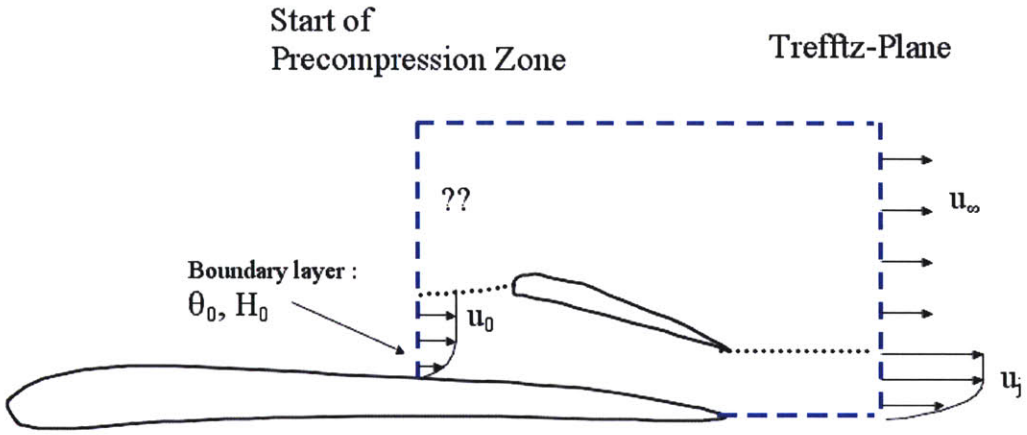

Figure 2-4: Inner control volume for an embedded engine

This problem has been addressed through the integrated control volume shown in Figure 2-5, where the flow that does not go through the engine is at freestream conditions at the control volume boundaries.

The thrust and drag need to be defined in a manner appropriate for the integrated control volume, because the force on the engine flow is partly due to the airframe. The flow that has been accelerated through the engine has a momentum excess (over the freestream momentum) at the Trefftz Plane. For the purpose of this study, this momentum excess at the Trefftz Plane will be called "net thrust". With the notations

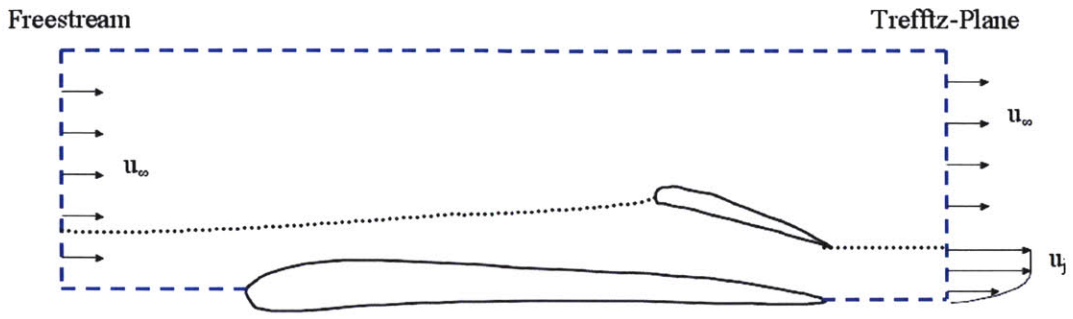

Figure 2-5: Outer control volume for an embedded engine

of Figure 2-5, the net thrust is:

$$T_N = \int_{\text{engine flow}} \rho(u_j - u_\infty)u_j \, \mathrm{d}A. \tag{2.15}$$

The "net drag" is the remainder of the momentum deficit at the Trefftz Plane, i.e. the bare airframe drag D_A plus the nacelle drag $D_{nacelle}$ minus the ingested drag D_w:

$$D_N = D_A + D_{nacelle} - D_w. \tag{2.16}$$

The ingested boundary layer flow contributes to the net thrust because it is accelerated by the engine. This boundary layer would have contributed to the bare airframe drag if it were not ingested by the engine. Neglecting the friction that would occur downstream of the start of the precompression zone, the ingested drag D_w can be calculated using a modified von Karman equation (Drela [14]):

$$D_w = \rho u^2 \theta b \left(\frac{u}{u_\infty}\right)^{H_{avg}}. \tag{2.17}$$

In equation (2.17), b is the span of ingested boundary layer, u_∞ is the freestream velocity, H_{avg} is the average value of the shape factor between the start of the precompression zone and the downstream wake, and all other quantities are calculated at the start of the precompression zone.

The momentum excess at the Trefftz Plane must balance the momentum deficit giving

$$T_N = D_A + D_{nacelle} - D_w. \tag{2.18}$$

The net drag, net thrust, ingested drag and bare airframe drag are shown in Figure 2-6. The main point is that the net thrust is neither constant with BLI nor equal to

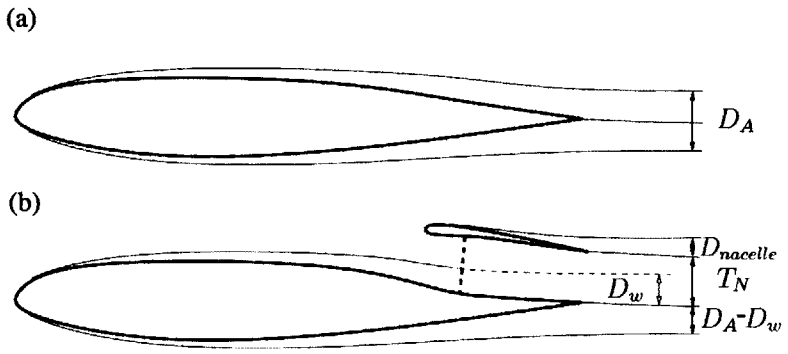

Figure 2-6: Drag and thrust definitions for an aircraft with embedded engines and BLI, adapted from Drela [14]
(a) bare airframe
(b) aircraft with embedded engines and BLI

the propulsive force provided by the engine[2]. It depends on the amount of ingested boundary layer and on the modifications of airframe drag associated with BLI. The utility of the net thrust comes from the fact that it can be linked with the airframe drag, the ingested drag, the freestream conditions and the engine flow properties at the start of the precompression zone and at the Trefftz Plane.

2.6 Comparison of podded and embedded engines

Once the features of the flow to be captured and the control volumes to be used have been defined, the method of comparison of podded and embedded engines needs to

[2]The propulsive force provided by the engine is equal to the sum of the bare airframe drag and nacelle drag and does *not* change with BLI

be determined. The baseline case is an airframe with podded engines and no BLI, and the comparison is for the same airframe with embedded engines. Since the net thrust changes with BLI, *the comparison will be done at constant airframe drag rather than constant net thrust.* The nacelle drag will be considered as constant and will be included in the term D_A from now on. Comparisons will be done for the same freestream conditions (Mach number, altitude), at top of climb, and with the same fan diameter for podded and embedded engines. The air is considered as a perfect gas with constant specific heats.

2.7 Figure of merit

The objective of this study is to compare the fuel burn $\dot{m}_f$ of a boundary layer ingesting propulsion system to that of a podded one. The fuel burn is linked to the thrust power by the following steps:

- Some fraction, $\eta_{combustion}$ (almost unity), of chemical energy is transformed into thermal energy in the combustor.
- Some fraction, η_{th}, of thermal energy is converted into mechanical energy (work).
- Some fraction, η_p, of the mechanical energy of the flow is used to provide thrust power.

For a high bypass ratio engine, most of the mechanical power is provided by the fan. Figure 2-7 illustrates this process and defines the efficiencies associated with each energy transformation.

Conventional figures of merit are propulsive efficiency and specific fuel consumption defined as follows (Cumpsty [5]):

$$\eta_p = \frac{\text{Power to aircraft}}{\text{Power to jet}} = \frac{T_N u_\infty}{\dot{m}_e \Delta KE}. \tag{2.19}$$

$$SFC = \frac{\text{Fuel burn}}{\text{Net thrust}} = \frac{\dot{m}_f}{T_N}. \tag{2.20}$$

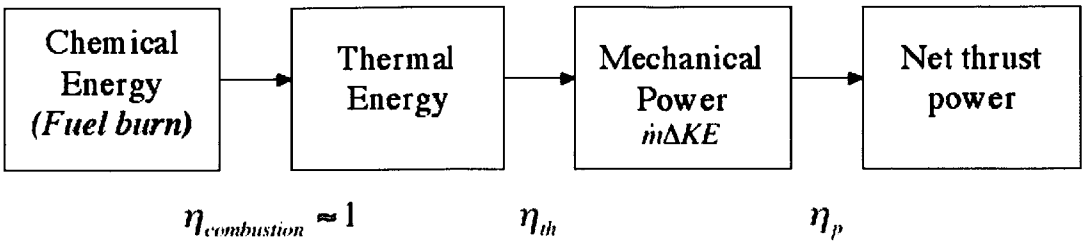

Figure 2-7: Process for the transformation of fuel burn into thrust power by the engine
η_{th} is the thermal efficiency.
$\eta_{mechanical}$ is the mechanical efficiency.
η_p is the propulsive efficiency.

However, the net thrust T_N decreases with boundary layer ingestion. A decrease in η_p or an increase in SFC will therefore not necessarily mean that there is an increase in fuel burn.

A better definition of propulsive efficiency is the ratio of useful power to the mechanical power as explained in Appendix A.

$$\eta_p = \frac{\text{Useful power}}{\text{Mechanical power}} = \frac{D_A u_\infty}{\dot{m}_e \Delta KE}. \tag{2.21}$$

Using this definition of the propulsive efficiency as a figure of merit is also misleading because η_p can be above one, so it does not measure how much energy is lost. As a result, a different metric is used here.

The thermal efficiency of the core engine is considered not to change with boundary layer ingestion, so fuel burn changes are directly linked with the changes in the power absorbed by the fan. A normalized fan power thus seems a more appropriate measure for assessing an engine's performance. To compare both propulsion systems, a power saving coefficient will be defined as follows.

$$PSC = \frac{P^* - P}{P^*}. \tag{2.22}$$

In equation (2.22), P^* is the fan power for podded engines, and P is the fan power with BLI for the same airframe drag, flight conditions, and fan diameter. The power saving coefficient is the figure of merit in this study.

2.8 Hierarchy of possible models

Different models can be developed to capture the flow characteristics that were described in Section 2.3. The simplest approach is to assume the flow is fully mixed before the engine (Rodriguez [31]) although this does not address any of the actual performance issues related to fan effect on inlet non-uniformity. The next level of modeling is a 1-D parallel compressor model, where the boundary layer is replaced by a stream of uniform properties. To account for non-mixing and losses, an integral boundary layer model can be used, based on the integral boundary layer equations (Drela [13]). The highest level of fidelity is 3-D calculations for viscous or inviscid flow through a straight or curved duct. In this thesis, the 3-D inviscid calculations for a straight duct are carried out using a body force code developed by Gong [18].

The different models are presented in Table 2.1. Those in italics were not implemented, but the others will be discussed in the subsequent chapters. (Rodriguez's model was described in Section 2.1.)

Table 2.1: Hierarchy of possible models for BLI

0-D	Mixed flow (Rodriguez)	Incomp.	Inviscid
1-D	Parallel compressor	Incomp.	Inviscid
1-D	Parallel compressor	Comp.	Inviscid
2-D	Boundary layer-like description (straight duct)	Comp.	Viscous
2-D	*Curved duct*	Comp.	Viscous
3-D	Straight duct	Comp.	Inviscid
3-D	*Straight duct*	Comp.	Viscous
3-D	*Curved duct*	Comp.	Viscous

2.9 Summary of the approach

The performance of an embedded engine with BLI will be estimated for a fan in a straight duct. The features of the flow that are included are the interaction of the airframe and the engine, boundary layer behavior in a duct, fan distortion transfer, fan performance, and duct losses. New definitions of thrust and drag have been developed. The performance of the embedded engine, represented through the power saving coefficient, will be compared to that of a podded engine for the same airframe drag, flight conditions and fan diameter.

Chapter 3

A parallel compressor treatment of BLI

A parallel compressor analysis of a ducted propulsor ingesting two uniform streams of different properties is described. The features captured in the analysis developed are non-complete mixing of the low stagnation pressure region and the freestream, influence of fan characteristics, effect of area changes on non-uniformities, and compression ahead of the duct.

3.1 Principle of the parallel compressor treatment

Parallel compressor models have been widely used to model compressor response to inlet distortion [4, 19, 28]. The concept is to represent a circumferential distortion by two uniform streams of different stagnation pressures, assuming no mixing between the two streams. The static pressure at the exit of the compressor can be considered as uniform across the duct if the exhaust duct is straight, of constant area, if the leaving (absolute) flow angle is uniform, and if the flow can be considered two-dimensional (Longley and Greitzer [28]). Each of the streams is assumed to operate at one point of the compressor map. The two local operating points are set by the downstream pressure, the mean flow and the stagnation pressure defect.

The parallel compressor model can be simply illustrated for incompressible flow. The compressor map can be represented as in Figure 3-1. The x-axis represents the flow coefficient.

$$\phi = \frac{u}{U}. \tag{3.1}$$

In equation (3.1), u is the velocity at the fan face and U is the fan tip speed. The y-axis represents the stage loading coefficient.

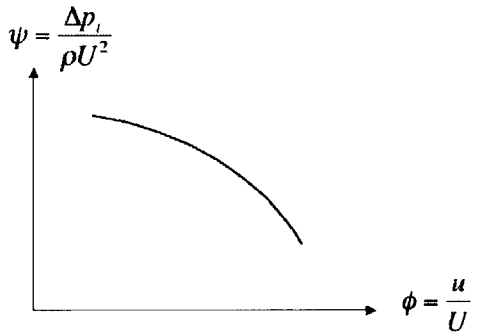

Figure 3-1: Incompressible compressor map

$$\psi = \frac{\Delta p_t}{\rho U^2}. \tag{3.2}$$

The axial velocity is constant across the compressor so Δp_t and Δp are the same.

The negative slope of the curve means there is a higher pressure rise across the compressor in the low velocity stream than in the high velocity stream. To achieve a uniform fan exit static pressure, the static pressure of the low speed stream at the compressor face must therefore be lower than that of the high velocity stream. This means the low velocity flow is accelerated upstream of the fan, with streamline curvature as sketched in Figure 3-2, so the non-uniformity is reduced. This characteristic of a compressor is described by Smith [36] as the "ability of a propulsor to add more energy to the low velocity parts of a wake and thus recover the flow to a more uniform state".

Figure 3-3 shows a parallel compressor graphical solution of compressor subjected to inlet distortion. The two operating points on the compressor map are seen. ψ_{TS} represents the exit static pressure minus inlet total pressure. ψ_{SS} is the exit static pressure minus the inlet static pressure. The figure also illustrates the loss in mean pressure rise due to inlet distortion.

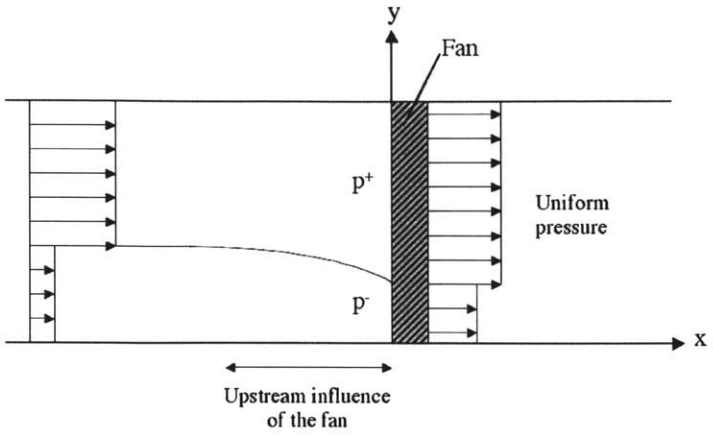

Figure 3-2: Sketch of a parallel compressor with streamline curvature ahead of the fan

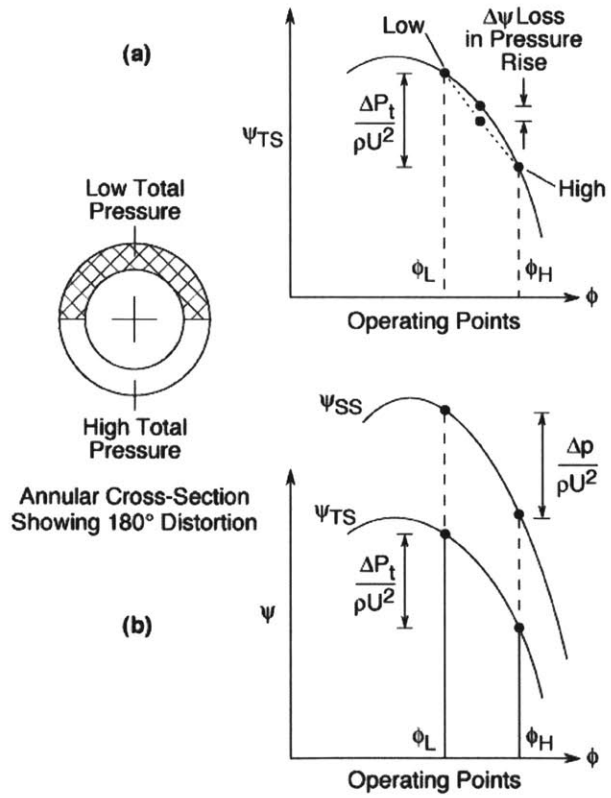

Figure 3-3: Parallel compressor model for a flow with circumferential distortion, taken from Longley and Greitzer [28]

3.2 Application to a ducted fan with boundary layer ingestion

The flow is assumed incompressible (constant and uniform density ρ) and inviscid throughout Section 3.2.

3.2.1 Non-dimensional parameters

Three groups of independent non-dimensional parameters characterize the problem.

- Aircraft parameters: aircraft drag coefficient $C_{D_A} = D_A/\frac{1}{2}\rho u_\infty^2 A_f$, aircraft and fan tip velocity ratio u_∞/U.
- Flow properties at the start of the precompression zone: local to freestream velocity ratio u_0/u_∞, boundary layer shape factor H_0, ingested drag D_w/D_A (or boundary layer momentum thickness)[1].
- Duct geometry: exhaust area ratio A_e/A_f.

The power saving coefficient is a function of all these independent parameters, which are assumed known from airframe calculations and preliminary engine design[2]. To make use of the parallel compressor model, the boundary layer is replaced by a uniform stream of velocity u_{0_2} and area A_{0_2} at the start of the precompression zone. The two boundary layer related non-dimensional parameters, H_0 and D_w/D_A, are therefore replaced by u_{0_2}/u_∞ and A_{0_2}/A_f.

3.2.2 Power for uniform flow (podded engines)

We consider an aircraft with podded engines as a baseline. To calculate the power to propel an aircraft with podded engines, one must determine the pressure rise across the fan and the mass flow (for uniform flow) in a ducted fan that achieves a given exit

[1]The parameter δ^*/δ is not used because the actual profile of the boundary layer is not of interest here. What matters is the momentum deficit and the blockage

[2]The parameters used in Section 3.2 are those of the first version of the Silent Aircraft's engine, GRANTA 252-R

momentum flux. A ducted fan is shown as constant area with a converging nozzle in Figure 3-4.

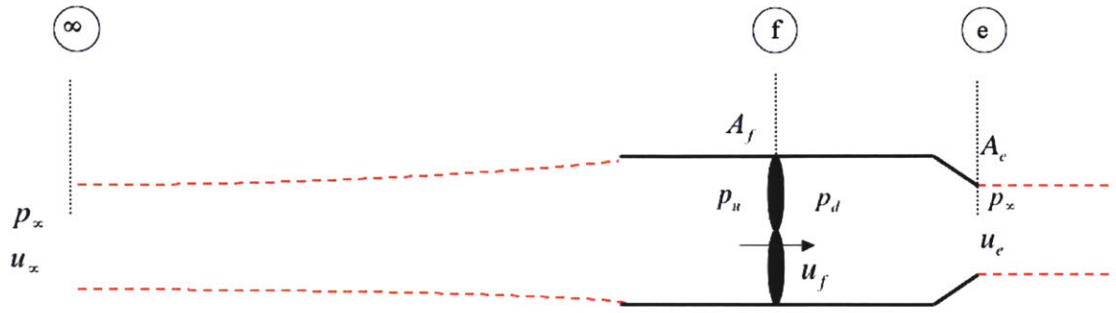

Figure 3-4: Schematic of a straight ducted fan with uniform flow

Continuity for the engine flow yields:

$$u_\infty A_\infty = u_f A_f = u_e A_e. \tag{3.3}$$

Bernoulli's equation can be applied to the incompressible and inviscid stream upstream and downstream of the fan:

$$p_\infty + \frac{1}{2}\rho u_\infty^2 = p_u + \frac{1}{2}\rho u_f^2, \tag{3.4}$$

$$p_d + \frac{1}{2}\rho u_f^2 = p_\infty + \frac{1}{2}\rho u_e^2. \tag{3.5}$$

The fan is assumed ideal here (neither losses nor deviation), so the compressor pressure rise is a straight line of slope t:

$$\frac{p_d - p_u}{\rho U^2} = 1 - t\frac{u_f}{U}. \tag{3.6}$$

The parameter t is related to the fluid outlet angles β_2 (from the rotor) and α_3 (from the stator).

$$t = \tan\alpha_3 + \tan\beta_2. \tag{3.7}$$

According to Horlock [22], the outlet angles, and thus t, "will vary little with changing inlet angles up to the stalling point of the cascades" and t will therefore be considered as constant.

Applying conservation of momentum and equating the net thrust to the airframe drag yields:

$$T_N = \rho u_e A_e (u_e - u_\infty) = D_A. \tag{3.8}$$

Solution of equations (3.3)-(3.8) gives the mass flow and the fan pressure rise for a podded ducted fan propelling an airframe of drag D_A. The fan power is equal to:

$$P^* = \dot{m} \frac{\Delta p}{\rho}. \tag{3.9}$$

3.2.3 Power for non-uniform flow (embedded engines with BLI)

The power for an engine with BLI and the power saving coefficient are now calculated. With boundary layer ingestion, the flow is no longer uniform. The nomenclature used in the description of the flow is indicated in Figure 3-5.

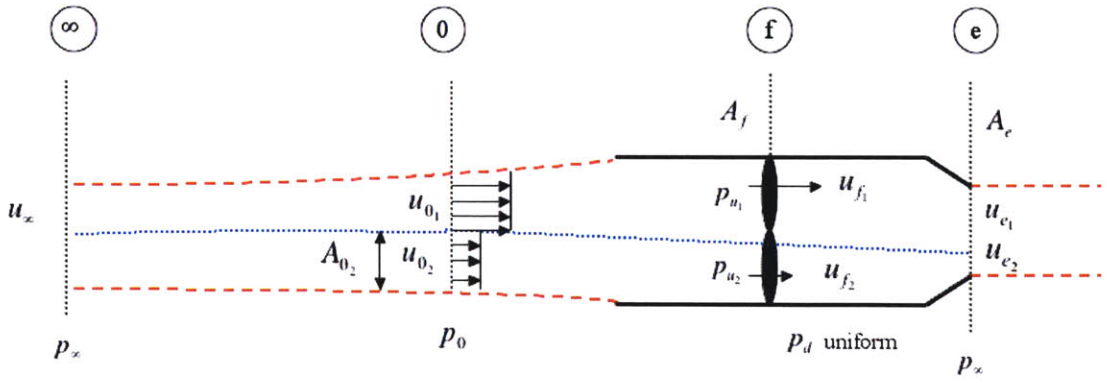

Figure 3-5: Schematic of a straight ducted fan with non-uniform flow

The characteristics u_{0_2} and A_{0_2} of the stream representing the boundary layer are

determined to match the boundary layer shape factor,

$$H_0 = \frac{\delta_0^*}{\theta_0} = \frac{u_0}{u_{0_2}}, \tag{3.10}$$

and to match the ingested drag expressed in equation (2.17), which is proportional to the momentum thickness θ_0. H_{avg} is taken to be $(H_0 + 1.0)/2$, 1.0 being the shape factor in the far wake.

$$\theta_0 = \frac{D_w}{\rho u_0^2}\left(\frac{u_\infty}{u_0}\right)^{H_{avg}} = \left(1 - \frac{u_{0_2}}{u_0}\right)\frac{u_{0_2}}{u_0}A_{0_2}. \tag{3.11}$$

Thus δ_0^* is also matched[3].

Continuity can be applied between the single stream at station ∞ and the two streams at station 0; for stream 1 and stream 2 between station 0 and station f; and for stream 1 and stream 2 between station f and station e. Bernoulli's equation can be applied between station ∞ and station 0 for the freestream; between station 0 and station f for both streams; and between station f and station e for both streams. The pressure rise across the fan for each stream is determined as for the uniform flow situation:

$$\frac{p_d - p_{u_1}}{\rho U^2} = 1 - t\frac{u_{f_1}}{U}. \tag{3.12}$$

$$\frac{p_d - p_{u_2}}{\rho U^2} = 1 - t\frac{u_{f_2}}{U}. \tag{3.13}$$

The net thrust is equal to the change in momentum flux of the engine flow. It is also equal to the airframe drag minus the ingested drag as given in Section 2.5:

$$T_N = D_A - D_w = \rho u_{f_1}(A_f - A_{f_2})(u_{e_1} - u_\infty) + \rho u_{f_2}A_{f_2}(u_{e_2} - u_\infty). \tag{3.14}$$

Solving the system of equations (3.12) to (3.14) and the continuity and Bernoulli's

[3]Note that other choices are possible. For example, the kinetic energy thickness or the energy factor could be matched. δ^* and H were chosen because they represent the mass flow defect and the state of the boundary layer

equations, the fan power is calculated in equation (3.15).

$$P = \rho u_{f_1}(A_f - A_{f_2})\frac{p_d - p_{u_1}}{\rho} + \rho u_{f_2} A_{f_2}\frac{p_d - p_{u_2}}{\rho}. \tag{3.15}$$

3.2.4 Results

Power saving coefficient

The first result concerns the power saving coefficient (PSC) which is shown as a function of ingested drag in Figure 3-6. All the other independent parameters presented in Section 3.2.1 are kept constant. The slope of the fan characteristic varies with D_w/D_A, because it is defined by the thrust requirement. In Figure 3-6 the PSC is positive, which means that less power is needed with BLI than without it. The plot shows a monotonic variation of the PSC indicating that the more boundary layer ingested, the better the performance.

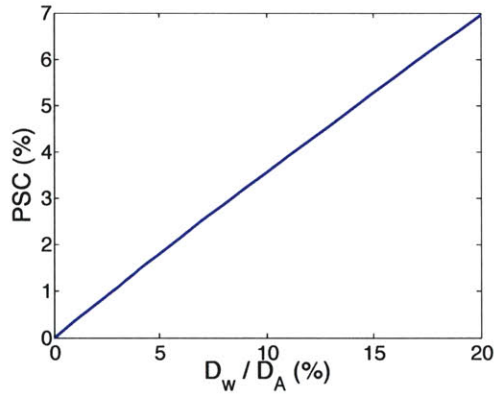

Figure 3-6: Power saving coefficient vs. ingested drag for incompressible flow in a ducted fan with BLI

Calculations were done for different values of u_∞/U, keeping u_0/u_∞ and u_{0_2}/u_∞ the same. The results are shown in Figure 3-7. They show an increase in the power saving coefficient with an increase of u_∞/U (or for constant flight speed, a decrease in fan tip speed). The trend of the power saving coefficient, however, remains the same.

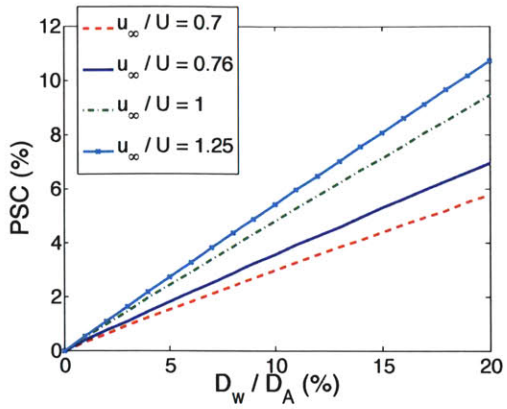

Figure 3-7: Evolution of the power saving coeffficient vs. ingested drag for different flight speed to blade tip speed ratios

Propulsive efficiency

As stated in Section 2.7, there is an ambiguity in using propulsive efficiency, defined as power to aircraft and power to jet ratio as in equation (2.19), as a figure of merit because a decrease in propulsive efficiency may not necessarily mean an increase in fuel burn,

$$\eta_p = \frac{\text{Power to aircraft}}{\text{Power to jet}} = \frac{T_N u_\infty}{\dot{m}_e \Delta KE}. \tag{2.19}$$

To illustrate this point, the propulsive efficiency η_p is plotted as a function of ingested drag in Figure 3-8. The propulsive efficiency decreases with ingested drag, although it was just shown that BLI results in power savings. This result occurs because there is a more rapid decrease in net thrust than in fan power.

A more appropriate definition of propulsive efficiency is the ratio of useful power to power to jet as explained in Appendix A:

$$\eta_p = \frac{\text{Useful power}}{\text{Power to jet}} = \frac{D_A u_\infty}{\dot{m}_e \Delta KE}. \tag{2.21}$$

The propulsive efficiency defined in equation (2.21), plotted in Figure 3-9, increases with increasing BLI.

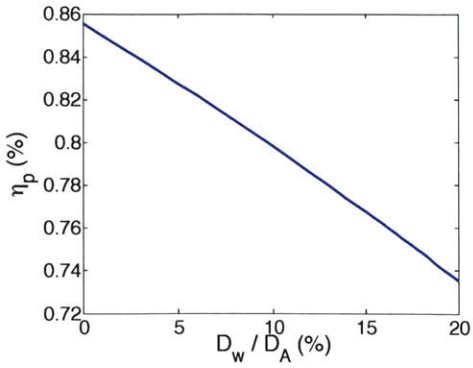

Figure 3-8: Propulsive efficiency $T_N u_\infty / \dot{m}_e \Delta KE$ vs. ingested drag for incompressible flow in a ducted fan with BLI

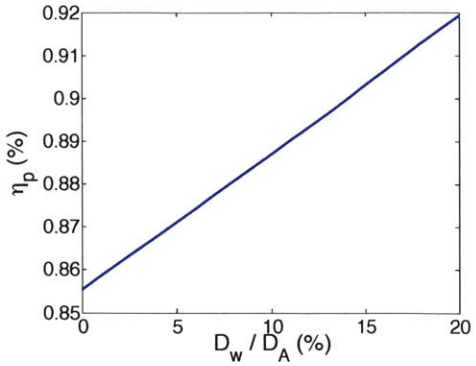

Figure 3-9: Propulsive efficiency $D_A u_\infty / \dot{m}_e \Delta KE$ vs. ingested drag for incompressible flow in a ducted fan with BLI

Mass flow

Another interesting result is the evolution of the normalized mass flow $\dot{m}/\rho u_\infty A_f$. This quantity decreases with boundary layer ingestion, which means that at constant fan diameter the physical mass flow decreases. The reason can be seen by considering the square wake presented in Chapter 1. For the embedded engine with BLI, the net thrust is:

$$T_N = \rho u_e A_e (u_e - u_\infty) \tag{3.16}$$

At constant exit diameter, the change in net thrust is related to the change in exit velocity by:

$$\mathrm{d}T_N = \rho A_e (2u_e - u_\infty)\, \mathrm{d}u_e \tag{3.17}$$

Since the net thrust decreases with BLI and since $u_e \geq u_\infty$, u_e, and thus the mass flow decreases with increasing BLI.

3.3 Effects of compressibility

Compressibility is now considered, keeping the assumption of inviscid flow. To account for the changes in area between the rotor face and the stator exit, the fan exit area A_d is now taken as different from the fan face area A_f.

3.3.1 Non-dimensional parameters

The non-dimensional parameters governing the compressible problem can be divided into four groups:

- Aircraft parameters: aircraft drag coefficient $C_{D_A} = D_A/\frac{1}{2}\rho_\infty u_\infty^2 A_f$, aircraft Mach number M_∞.
- Flow properties at the start of the precompression zone: local Mach number M_0, boundary layer shape factor H_0, boundary layer energy factor H_0^*, ingested drag (or boundary layer momentum thickness) D_w/D_A.
- Duct geometry: fan exit to fan face area ratio A_d/A_f.
- Fan parameters: fan characteristic (pressure ratio and efficiency as a function of corrected mass flow).

The power saving coefficient is a function of all these independent parameters, which are known from airframe calculations and from preliminary engine design[4]. In contrast to the incompressible problem, the exhaust area is set by choking conditions at the nozzle, so it cannot be chosen independently. For the compressible parallel compressor model, the boundary layer is replaced by a uniform stream of Mach number M_{0_2}, stagnation pressure $p_{t_{02}}$, and area A_{0_2} at the start of the precompression zone. The three boundary layer related non-dimensional parameters H_0, H_0^*, and D_w/D_A are therefore replaced by M_{0_2}, $p_{t_{02}}/p_\infty$ and A_{0_2}/A_f.

3.3.2 Calculation of flow and fan power for non-uniform flow

The calculation procedure is based on a compound-compressible flow analysis (Greitzer et. al. [20])[5]. At station 0, the boundary layer is replaced by a uniform stream of Mach number M_{0_2}, stagnation pressure $p_{t_{02}}$, and area A_{0_2}. These quantities are

[4]The parameters used in Section 3.3 are those of the first version of the Silent Aircraft's engine, GRANTA 252-R

[5]Note that in [20], the static pressure is assumed uniform across the duct, which is *not* the case at the fan face in this problem

determined to match the shape factor, the ingested drag, and the mass average stagnation pressure of the flow. This average is calculated by assuming a Coles profile [13] for the boundary layer and uniform static pressure (see Appendix B for more details on the Coles profile.)

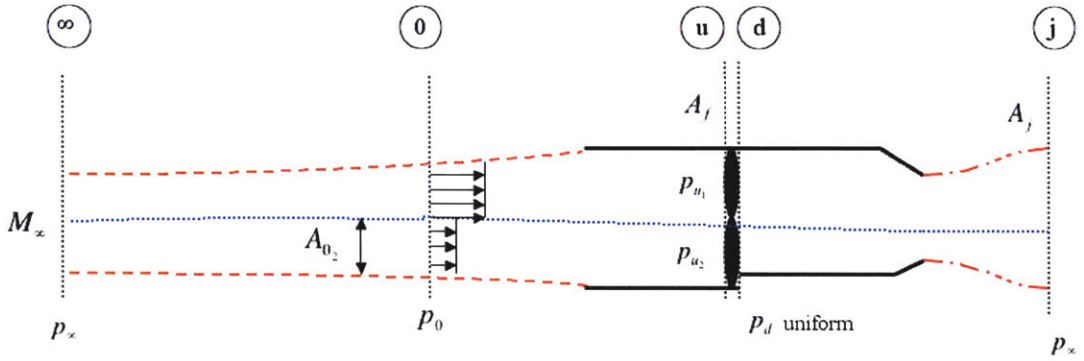

Figure 3-10: Schematic of a straight ducted fan with non-uniform compressible flow and a choked nozzle

To calculate the flow from station 0 to j (as shown in Figure 3-10), one can start with an initial guess of the mass flow $\dot{m}_1$ of the high stagnation pressure stream. There is no mixing between the two flows, $\dot{m}_1$ and $\dot{m}_2$ remain constant in the entire duct, and the stagnation pressure does not change in each stream from station 0 to station u (fan face). The stagnation temperature is taken as uniform upstream of the fan. Thus, p_t and T_t are known at station 0 and u. They can be calculated at the fan exit from the fan equations. The pressure ratio across the fan is a function of the corrected mass flow at the fan face:

$$\Pi_k = \frac{(p_{t_k})_{fan\ exit}}{(p_{t_k})_{fan\ face}} = f\left(\frac{\dot{m}_k\sqrt{T_{t_k}/T_{ref}}}{p_{t_k}/p_{ref}}\right)_{fan\ face} \quad \text{for each stream.} \tag{3.18}$$

The efficiency of the fan is also a function of the corrected mass flow at the fan face:

$$\eta_k = g\left(\frac{\dot{m}_k\sqrt{T_{t_k}/T_{ref}}}{p_{t_k}/p_{ref}}\right)_{fan\ face} \quad \text{for each stream.} \tag{3.19}$$

The temperature ratio can be calculated from the definition of isentropic efficiency:

$$\tau_k = \frac{(T_{t_k})_{fan\ exit}}{(T_{t_k})_{fan\ face}} = 1 + \frac{\Pi_k^{(\gamma-1)/\gamma} - 1}{\eta_k} \quad \text{for each stream.} \tag{3.20}$$

The stagnation pressures p_{t_1} and p_{t_2}, and the stagnation temperatures T_{t_1} and T_{t_2} are now known at the fan exit. They are constant from station d (fan exit) to station j. Thus, p_t and T_t are known at every station for each stream.

At each station, the corrected flow per unit area can be expressed as a function of Mach number for each stream:

$$\frac{\dot{m}_k\sqrt{RT_{t_k}}}{p_{t_k}A_k\sqrt{\gamma}} = D(M_k) = M_k\left(1 + \frac{\gamma-1}{2}M_k^2\right)^{-\frac{\gamma+1}{2(\gamma-1)}}. \tag{3.21}$$

Three other equations are applicable:

$$\frac{p_{t_k}}{p_k} = \left(1 + \frac{\gamma-1}{2}M_k^2\right)^{\frac{\gamma}{\gamma-1}} \quad \text{for both streams,} \tag{3.22}$$

$$A = A_1 + A_2. \tag{3.23}$$

At the fan exit, the static pressure is uniform across the duct, and the previous five equations (3.21) - (3.23) can be solved for $p_1 = p_2$, A_1, A_2, M_1 and M_2. Likewise, at station j, the static pressure is uniform and equal to p_∞. Equation (3.22) for each stream at station j yields M_1 and M_2 at the jet. Applying equation (3.21) gives A_1 and A_2 at the jet. The velocity can then be determined from the Mach number and the stagnation temperature, and finally the jet momentum flux and net thrust can be calculated. The mass flow can then be iterated to achieve the required momentum

flux. The fan power is:

$$P = \dot{m}_1 c_p \left(T_{t_{d_1}} - T_{t_{u_1}} \right) + \dot{m}_2 c_p \left(T_{t_{d_2}} - T_{t_{u_2}} \right). \tag{3.24}$$

For uniform flow, the same equations apply for only one stream.

3.3.3 Results

Power saving coefficient

Figure 3-11 presents the power saving coefficient for compressible flow through an ideal fan. The Mach number at the start of the precompression zone is $M = 0.94$ (Freuler [17]). The results have the same trends as those of the incompressible model which are also shown. The power savings are positive for BLI, and they increase with ingested drag. However, the savings are lower than those obtained with the incompressible model.

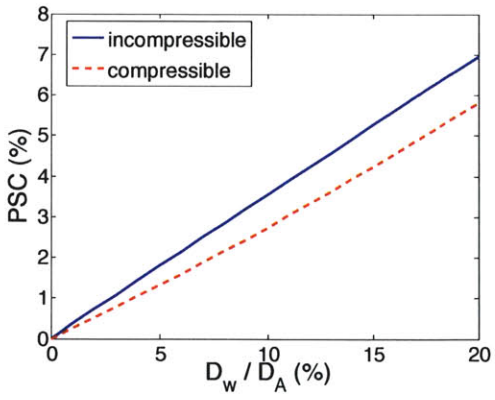

Figure 3-11: Power saving coefficient vs. ingested drag for compressible flow in a ducted fan with BLI

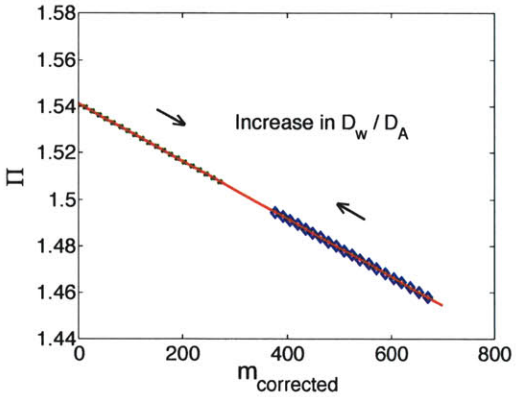

Figure 3-12: Operating points on the fan compressor map for different values of D_w/D_A
The x-axis is the corrected mass flow $\dot{m}_{corrected} = \dot{m}\frac{\sqrt{T_t/T_{ref}}}{p_t/p_{ref}}$. The y-axis is the pressure ratio Π.

The fan characteristic and the two local operating points are shown for different levels of D_w/D_A in Figure 3-12. The ideal fan characteristic used is an approximation

of the generic fan characteristic used for the initial designs of the Silent Aircraft's engine.

Results for a non-ideal fan were also obtained. The efficiency (a parabola) and the non-ideal fan characteristic are shown in Figures 3-13 and 3-14. The power saving

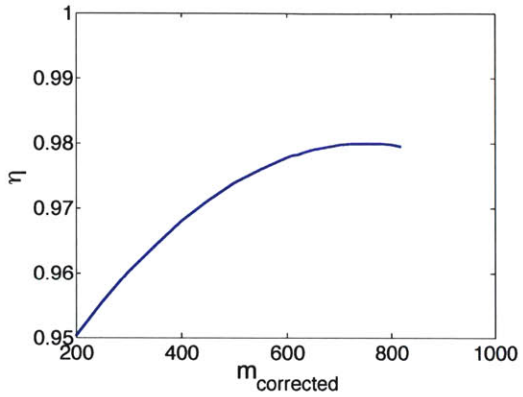

Figure 3-13: Efficiency vs. corrected mass flow $\dot{m}_{corrected} = \dot{m}\frac{\sqrt{T_t/T_{ref}}}{p_t/p_{ref}}$

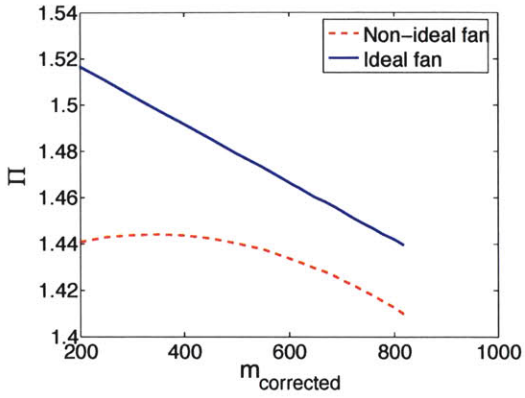

Figure 3-14: Compressor map for ideal and non-ideal fans
The x-axis is the corrected mass flow $\dot{m}_{corrected} = \dot{m}\frac{\sqrt{T_t/T_{ref}}}{p_t/p_{ref}}$. The y-axis is the pressure ratio Π.

coefficient obtained for this fan characteristic is shown in Figure 3-15. It is slightly lower than that obtained for the ideal fan, but the trend remains the same.

3.4 Conclusions on the parallel compressor models

The parallel compressor models are simplistic but they are useful for several reasons. They show there are power savings with boundary layer ingestion, and that these increase with BLI. The general trend implies that the engine installation should be such that it ingests as much boundary layer as possible at the trailing edge. It is therefore better to have a higher number of engines of smaller diameter spread out on the fuselage surface. In the next chapter, the effect of the assumptions made are examined.

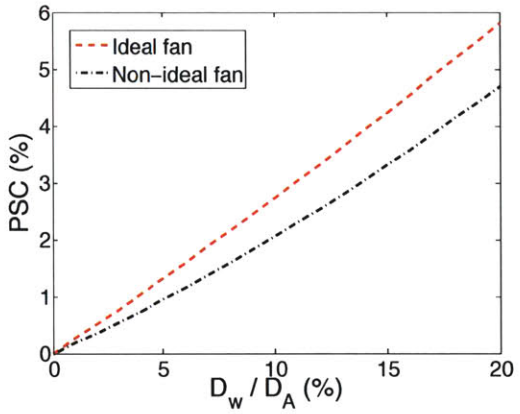

Figure 3-15: Power saving coefficient vs. ingested drag for compressible flow in a ducted non-ideal fan with BLI

Chapter 4

An integral boundary layer description of a ducted fan with BLI

The model presented in this chapter is based on integral boundary layer equations (Drela [13]), which are used to calculate the boundary layer integral properties and the inviscid core flow properties at any point in the duct. The approach accounts for non-complete mixing (and estimates for the rate of mixing), boundary layer behavior in a duct, fan characteristics, and inlet and exhaust losses.

The integral boundary layer equations (IBLE), derived in Appendix C, are a set of three equations representing continuity and conservation of momentum for the fluid in the boundary layer, and continuity for the entire flow. They have been used extensively by Drela [11, 12, 13] to quantify viscous - inviscid interaction in 2-D ducts. If the stagnation pressure, the stagnation temperature, the initial conditions (u_0, θ_0, and δ_0^*), and the area variation versus x are known, the solution of the IBLE gives the momentum thickness θ, the displacement thickness δ^* and the inviscid velocity u at any location x in the duct. The assumptions in the equations are:

- The flow can be represented by a boundary layer and an inviscid stream of

uniform properties at any duct location.

- The static pressure is uniform across the duct.
- Only integral descriptions of the boundary layer are needed, because only the fan pressure rise and the momentum flux at the exit are required to calculate the thrust and the power.

4.1 Application to a ducted fan with BLI

The flow is assumed compressible and the boundary layers turbulent[1] throughout Chapter 4.

4.1.1 Flow domain and non-dimensional parameters

The flow domain and the nomenclature used are shown in Figure 4-1. There is a core

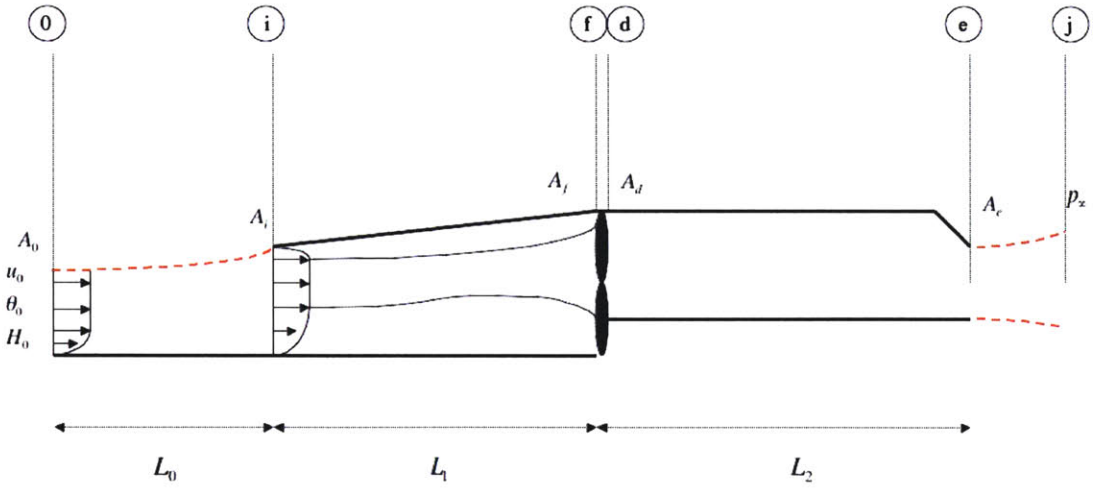

Figure 4-1: Schematic of a straight ducted fan with non-uniform compressible flow

stream of uniform velocity that will be referred to as "inviscid" stream in Chapter 4. The flow can be viewed as having two boundary layers of different thicknesses. One

[1]According to Drela [15], this should be the case for the boundary layer ingested by the Silent Aircraft's engines and the boundary layer which develops in the duct

boundary layer starts at the beginning of the inlet duct. The other is the boundary layer ingested from the fuselage. The first is referred to as the "thin" boundary layer and the second as the "thick" boundary layer throughout Chapter 4.

The independent non-dimensional parameters can be divided into four groups as for the parallel compressor models:

- Aircraft parameters: aircraft drag coefficient $C_{D_A} = D_A/\frac{1}{2}\rho_\infty u_\infty^2 A_f$, aircraft Mach number M_∞.
- Flow properties at the start of the precompression zone: local Mach number M_0, boundary layer shape factor H_0, ingested drag (or boundary layer momentum thickness) D_w/D_A.
- Duct geometry: inlet area ratio A_i/A_f, fan exit to fan face area ratio A_d/A_f, precompression length to fan face diameter ratio L_0/D_f, inlet length to fan face diameter ratio L_1/D_f, exhaust length to fan face diameter ratio L_2/D_f.
- Fan parameters: fan characteristic given by the pressure ratio and the efficiency as a function of corrected mass flow.

There are more non-dimensional parameters than for the parallel compressor model (Section 3.3.1) because of viscous effects: L_0, L_1, L_2 and A_i are now important.

The power saving coefficient is a function of all these independent parameters[2].

4.1.2 Modeling issues

The approach in modeling the ducted fan with BLI using the IBLE is not straightforward and a number of issues appear.

Boundary layers

The first issue arises in modeling the boundary layers. The model implemented here is quasi-two-dimensional, implying that both boundary layers will have the same lateral

[2]The parameters used in Chapter 4 are those of the first version of the Silent Aircraft's engine, GRANTA 252-R

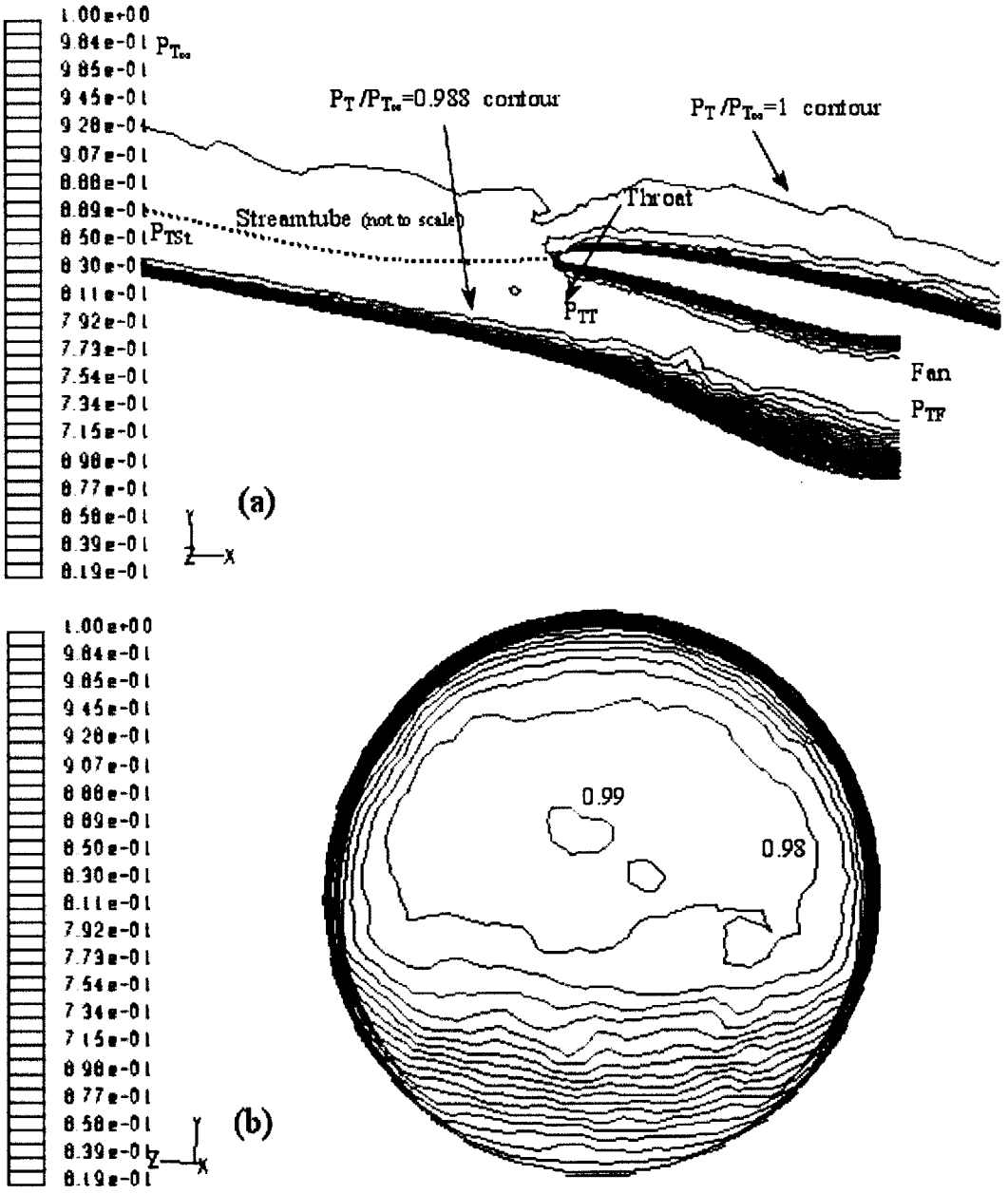

Figure 4-2: Stagnation pressure profile at the fan face for an inlet with boundary layer ingestion, taken from Freuler [17]

(a) Center section and (b) fan face stagnation pressure p_t/p_{t_∞}, contours (interval: 0.01) for inlet v1.1

extent. In reality, the lateral extent of the "thin" boundary layer is larger than that of the "thick" one, as shown in Figure 4-2, which portrays the distortion at the fan face for an initial inlet design of the Silent Aircraft.

Precompression zone

A second modeling issue arises in describing the behavior of the flow from station 0 to station i in Figure 4-1. There is a deceleration between these stations. The length over which this occurs and the distribution of the pressure in this region is not known a priori and cannot be found from a one-dimensional analysis. The approach here is to assume exponential decay, with a length scale of two inlet heights.

Fan - boundary layer interaction

A third modeling issue arises in modeling the interaction of the compressor with the flow non-uniformity, or distortion, i.e., the "distortion transfer" from upstream to downstream. The IBLE are based on the assumption of uniform static pressure across the duct, in other words they assume no streamline curvature. In reality, there will be an upstream (and downstream) non-uniform static pressure field due to the non-uniform flow into the fan. The distance over which this streamline curvature occurs is of the order of the non-uniformity length scale[3]. The static pressure field can change the thickness of the boundary layer. The distance over which the change occurs is small compared with the boundary layer development length so there is little effect on the overall entropy rise in the duct. However, to estimate the boundary layer properties downstream of the fan, the change in boundary layer thicknesses (or shape factor) across the fan needs to be known.

A number of approaches using integral methods have been applied to the computation of rotor (and compressor) casing boundary layers. Correlations and three-dimensional computations are the two approaches that appear to be used in industry. As described by Cumpsty [23], the tip clearance and the operating point of the fan

[3]This phenomenon is similar to a shear flow passing through a screen (Greitzer et. al. [20])

appear to be the major influences on the downstream boundary layer displacement thickness. However no general rule is shown by Cumpsty to calculate the downstream properties of the boundary layer, and the data are for boundary layers much thinner than the ones that are encountered with BLI. Cumpsty's results cannot thus be expected to apply.

A useful approach to estimating this effect for boundary layers has been put forward by Drela [12] in the context of flow through a duct with a heat exchanger, modeled as an actuator disk. He used exponential decay of the pressure difference between the freestream p_1 and the wall p_2, over a distance based on the boundary layer thickness. A conceptual picture of the streamlines and pressure field of the boundary layer entering and leaving the heat exchanger is shown in Figure 4-3. The pressure field due to the heat exchanger was reflected in an extra term in the integral momentum equation and the scheme worked well. For a fan, however, this approach, and the identification of the appropriate wall pressure and length scales are more difficult to apply.

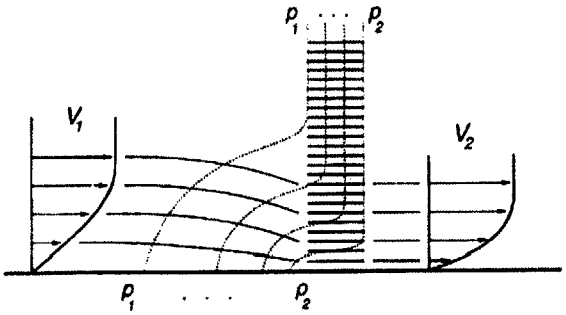

Figure 4-3: Pressure field contours and streamlines for a boundary layer approaching a heat exchanger, taken from Drela [12]

The approach in this thesis is to describe the boundary layer change across the fan parametrically. The downstream displacement and momentum thicknesses of the boundary layer normalized by the exit fan area A_d are given by k times the upstream

thicknesses normalized by the fan face area A_f:

$$\frac{\delta_d^*}{A_d} = k\frac{\delta_u^*}{A_f}, \tag{4.1}$$

$$\frac{\theta_d}{A_d} = k\frac{\theta_u}{A_f}. \tag{4.2}$$

The shape factor is assumed to remain the same across the fan. The parameter k is varied from 0.5 to 2.

This study is similar to the approach of Smith [36], who defined a recovery factor R as:

$$R = 1 - \frac{V_j - V_{j_w}}{V_0 - V_w}. \tag{2.1}$$

He assumed the recovery factor was the same for all streamlines. Integrating equation (2.1) over the boundary layer thickness leads for incompressible flow,

$$V_j\delta_j^* = (1 - R)V_0\delta_0^*. \tag{4.3}$$

Changing the constant k defined in equations (4.1) and (4.2) is thus similar to changing R as Smith did.

Fan pressure rise

The next issue concerns the calculation of the pressure rise. The fan will be assumed ideal, lossless, and with no deviation, e.g. the flow follows the blade metal angle. The stagnation pressure rise can only be calculated on an overall basis, i.e. based on the corrected flow. However, the pressure rise cannot be imposed in the boundary layer, since the downstream properties of the boundary layer depend on the edge velocity and stagnation properties. The assumption made here is to calculate the pressure and temperature rise in the inviscid part of the flow based on the corrected mass flow for this stream, and to let the pressure rise in the boundary layer come out of the calculation. The static pressure downstream of the fan is calculated from the inviscid flow characteristics.

4.1.3 Power for non-uniform flow

The power for a ducted fan with BLI is now calculated using the assumptions described above. At station 0 the Mach number M_0 of the inviscid flow is known and the stagnation pressure and temperature are assumed at freestream values. The shape factor H_0 and the ingested drag D_w are known. Equations (4.4) and (4.5) give δ_0^* and θ_0.

$$\theta_0 = \frac{D_w}{\rho_0 u_0^2}\left(\frac{u_\infty}{u_0}\right)^{(H_0+1)/2}. \tag{4.4}$$

$$\delta_0^* = H_0\theta_0. \tag{4.5}$$

To calculate the flow from station 0 to station j, one starts with an initial guess of the mass flow $\dot{m}$ which leads A_0. The IBLE are applied from station 0 to station i (precompression region), assuming an exponential area variation from A_0 to A_i and a length L_0 of two inlet heights, and give δ_i^*, θ_i, u_i. Assuming no change in stagnation pressure and temperature in the inviscid flow, the Mach number, static pressure and temperature can be calculated at station i. Two equations are added to the IBLE from station i to station u (inlet duct) to account for the "thin" boundary layer developing on the upper duct. The same procedure as for the precompression region is then applied and the flow properties at the fan face are known.

At the fan face, a Coles profile is assumed for the boundary layer (see Appendix B for more details on the Coles profile). This gives the boundary layer thickness δ and thus the mass flow of the inviscid part of the flow $\dot{m}_{inviscid}$. The corrected flow of the inviscid stream is defined as:

$$\dot{m}_{corrected} = \frac{\dot{m}_{inviscid}\sqrt{T_{t_f}/T_{ref}}}{p_{t_f}/p_{ref}}. \tag{4.6}$$

In equation (4.6) T_{t_f} is the stagnation temperature and p_{t_f} the stagnation pressure of the inviscid part of the flow at the fan face. The stagnation pressure p_{t_d} and temperature T_{t_d} of the inviscid part of the flow are then calculated from the fan characteristic. The properties of the boundary layer are assumed unchanged across

the fan, in other words, the thicknesses of the boundary layers normalized by the duct area are unchanged,

$$[\delta_d^*,\, \theta_d]\,/A_d = [\delta_u^*,\, \theta_u]\,/A_f. \tag{4.7}$$

From T_{t_d}, p_{t_d}, δ_d^* and A_d, the velocity u_d can be known. The same procedure as for the inlet is then applied from station d to station e. The area A_e is changed to achieve a choked nozzle.

The flow expansion between stations e and j is calculated using Squire equation (Schlichting [34]):

$$\theta_j = \theta_e \left(\frac{u_e}{u_j}\right)^{\frac{H_e+5}{2}}. \tag{4.8}$$

The net thrust is:

$$T_N = \dot{m}(u_j - u_\infty) - \rho_j u_j^2 \left(\theta_j^{top} + \theta_j^{bottom}\right). \tag{4.9}$$

The mass flow is changed until the required net thrust is achieved.

The stagnation temperature is assumed uniform across the boundary layer, so the fan power is:

$$P = \dot{m} c_p (T_{t_d} - T_{t_u}). \tag{4.10}$$

4.1.4 Power for uniform flow

For podded engines, the same procedure can be applied from station i (inlet) to station j (Trefftz Plane). There is no friction in the precompression region so a one-dimensional analysis can be used to determine the flow at the inlet. The parameters of Section 4.1.1 are unchanged except for the inlet to fan face area ratio A_i/A_f which is set equal to one for a podded inlet (constant area inlet duct), the inlet length to fan diameter ratio L_1/D_f, and the exhaust length to fan face diameter ratio L_2/D_f which are both taken to be 1. This gives an engine length of two fan diameters, in contrast to seven for the embedded case.

4.1.5 Results

Power saving coefficient

The power saving coefficient as a function of levels of boundary layer ingestion is shown in Figure 4-4[4]. The abscissa is the ratio of the ingested drag to the bare

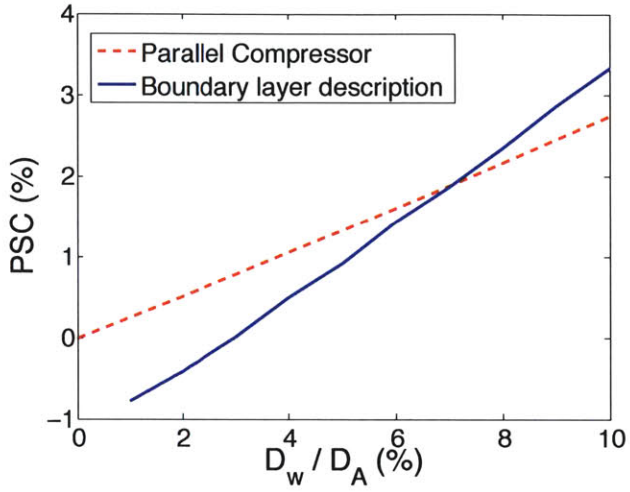

Figure 4-4: Power saving coefficiency vs. ingested drag for compressible flow in a ducted fan with BLI
The red dotted line corresponds to the PSC for the compressible parallel compressor model, the blue plain line to the PSC for the integral boundary layer description.

airframe drag and the ordinate is the per cent power saving compared to the podded inlet. The same fan characteristic as for the parallel compressor model (Section 3.3) was used. The curve obtained using the parallel compressor model is also shown for comparison. As with the parallel compressor model the PSC is positive, which means BLI is beneficial, and increases with BLI. There are 3.3% power savings when ingesting 10% airframe drag.

[4]The curve does not go to zero when D_w/D_A goes to zero, because it approaches the ratio between the power required for flow with thin boundary layers in a long (7 fan diameters) diverging ducted fan (embedded engine without BLI), and the power required for flow with thin boundary layers in a short (two fan diameters) constant area ducted fan (podded engines without BLI). This ratio is negative

Evolution of the boundary layer in the duct

The evolution of the boundary layer displacement thickness is shown in Figure 4-5. δ^* increases in the precompression zone and in the inlet because there is an adverse pressure gradient (diverging duct). Downstream of the fan δ^* decreases slightly in the straight duct and more in the nozzle. According to Drela [16], the reason for the

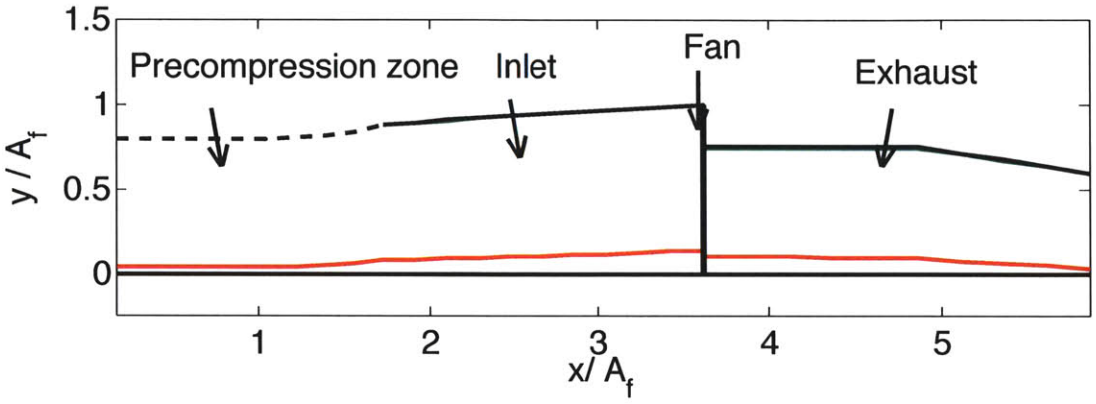

Figure 4-5: Evolution of the boundary layer displacement thickness in the ducted fan

The red line represents the "thick" boundary layer, the green line the "thin" boundary layer, the black plain line represents the duct, and the black dotted line represents the streamtube in the precompression region[5].

decrease of the boundary layer displacement thickness downstream of the fan is the following. The boundary layer is close to separation upstream of the fan. When the flow undergoes a less adverse pressure gradient as it is the case downstream of the fan (straight duct of constant area), the inviscid flow tends to "fill in" the boundary layer, as shown in Figure 4-6, and the boundary layer displacement thickness decreases. Wall shear stress, however, implies that the momentum thickness must increase, as the first equation (C.11) of the integral boundary layer equations shows:

$$\frac{\mathrm{d}\theta}{\mathrm{d}x} = \frac{C_f}{2} - (H + 2 - M_E^2)\frac{\theta}{u_E}\frac{\mathrm{d}u_E}{\mathrm{d}x}. \tag{C.11}$$

[5] A_f is an area per unit depth in the integral model, so x/A_f and y/A_f are non-dimensional quantities

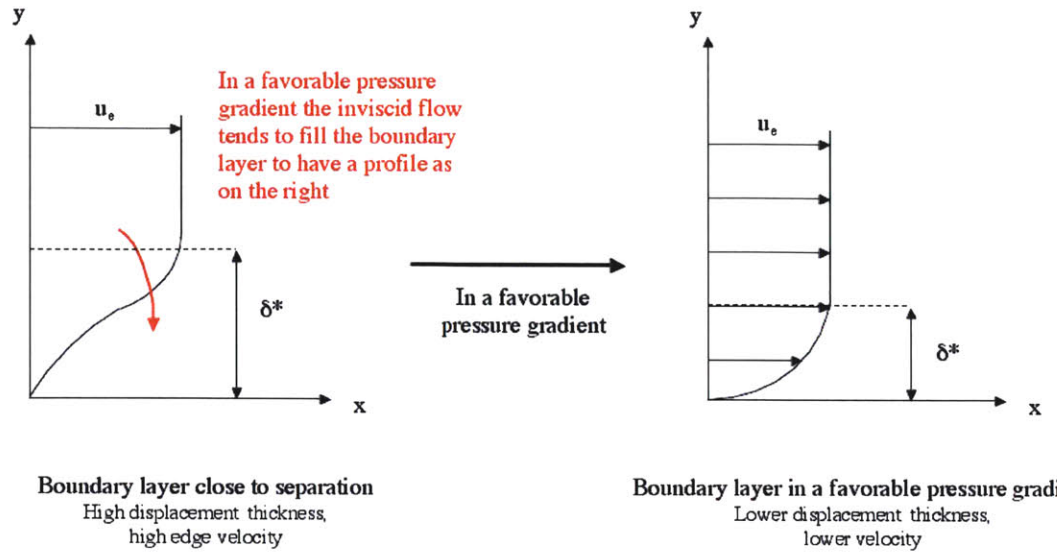

Figure 4-6: Explanation of the decrease of the boundary layer displacement thickness downstream of the fan

The displacement thickness depends not only on wall shear stress, but also on the dissipation coefficient and the energy factor.

Losses

The metric for duct losses is entropy generation. For adiabatic flows with no shaft work (Greitzer et. al. [20]),

$$\dot{S}_{total} = \dot{m}\overline{\Delta s}^{M} = -R\int \ln\left(\frac{p_{t_2}}{p_{t_1}}\right) \mathrm{d}\dot{m}. \tag{4.11}$$

In equation (4.11) $\overline{\Delta s}^{M}$ is the difference of mass average entropy between two locations 1 and 2 in the duct; $\dot{S}_{total}$ is the total entropy generation between the two locations. The boundary layer is approximated as a Coles profile and the stagnation pressure at a location y in the boundary layer is:

$$p_t(y) = p_f \left(\frac{T_{t_\infty}}{T_{t_\infty} - \frac{u(y)^2}{2c_p}}\right)^{\frac{\gamma}{\gamma-1}}. \tag{4.12}$$

The entropy generation is increased by a factor of 5.7 from no boundary layer ingestion to 10% ingested drag.

For the ducted fan without BLI the integral boundary layer formulation is within 6% of the simple estimate given by Denton [8]. This is seen in Figure 4-7 which gives a comparison of the calculated entropy production with the Denton formula [8]:

$$\dot{S}_{total} = \int_0^L C_D \frac{\rho_E u_E^3}{T_E} \, \mathrm{d}x, \tag{4.13}$$

where ρ_E, u_E, T_E are the edge density, velocity and static temperature, C_D is the dissipation coefficient, and L is the length of the duct. The difference between the

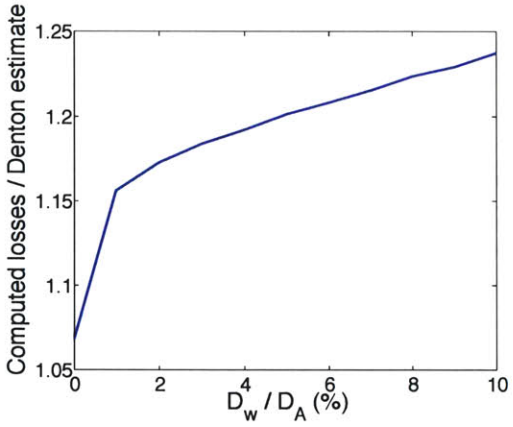

Figure 4-7: Comparison of obtained duct losses $\dot{S}_{total}$ with Denton estimate

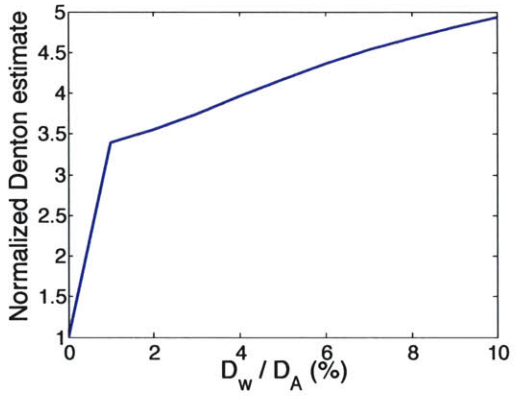

Figure 4-8: Denton estimate of entropy generation in the inlet

Denton estimate and the integral boundary layer formulation increases with BLI and is roughly 24% at 10% ingested drag. The difference can be explained by the approximations made in calculating the losses using the integral boundary layer model. A Coles profile was assumed for the boundary layer to calculate the losses using equation (4.11). However, after going through an adverse pressure gradient in the inlet, the boundary layer at the fan face is close to separation, and a Coles profile is not a good approximation[6]. The Denton estimate seems therefore a better estimate for

[6]The "jump" in the curve from 0% to 1% ingested drag comes from the fact that the limiting

losses. Figure 4-8[7] shows the Denton estimate. The entropy generation is multiplied by roughly 5 from no boundary layer ingestion to 10% ingested drag, partly because of the increase in edge velocity with BLI, but mostly because of the increase in duct length. The losses increase with BLI, but do not change the trends of the power saving coefficient.

Inlet performance is typically measured through a pressure recovery defined as:

$$\Pi = \frac{\overline{p_t}^M_{fan}}{\overline{p_t}^M_{inlet}}. \tag{4.14}$$

In equation (4.14) $\overline{p_t}^M$ is the mass average stagnation pressure. To calculate the average stagnation pressure, a Coles profile (see in Appendix B) is assumed. The mass average stagnation pressure is:

$$\overline{p_t} = \frac{1}{\dot{m}} \left[\int_0^\delta p \left(1 + \frac{\gamma - 1}{2} \frac{u^2}{\gamma R \left(T_{t_E} - \frac{u^2}{2c_p} \right)} \right) \rho_E u \, \mathrm{d}y + p_{t_E} \rho_E u_E (A - \delta) \right], \tag{4.15}$$

where ρ_E, u_E, p_{t_E}, T_{t_E} are the edge density, velocity, stagnation pressure and temperature, and p is the static pressure. The pressure recovery does not depend much on the ingested drag. The decrease in inlet pressure recovery between 1% and 10% BLI is roughly 0.25%.

Blockage

A blockage factor B can be defined as the ratio of the blocked area A_B to the duct area A (Johnston [24]). The blocked area is:

$$A_B = \int_0^A \left(1 - \frac{\rho u}{\rho_E u_E} \right) \mathrm{d}A = \delta^*, \tag{4.16}$$

situation is a long embedded engine without BLI (thin boundary layers that develop upstream of the engine). This produces more losses than the podded case

[7]Again, the jump is due to the trend of the model as D_w/D_A goes towards zero. The length and thus the Denton estimate for the losses is larger for the limit of the model as D_w/D_A goes to zero (embedded engine without BLI) than for the baseline (podded engine without BLI)

where ρ_E and u_E are the edge density and velocity. The blockage factor is therefore:

$$B = \frac{A_B}{A} = \frac{\delta^*}{A}. \tag{4.17}$$

The blockage depends much more strongly on the ingested drag than the loss. Blockage at the fan face is increased by more than 100 from no BLI to 10% BLI. This is explained by analyzing the dependence of the losses and the blockage on the boundary layer thickness. Equation (4.17) shows that the blockage is directly proportional to δ^*. However the losses scale as:

$$\dot{S} = \int_0^L \frac{C_D \rho_E u_E^3}{T_E} \, \mathrm{d}x = \int_0^L \frac{C_D \rho_E}{T_E} \left(\frac{\dot{m}}{\rho_E (A - \delta^*)} \right)^3 \mathrm{d}x \sim C_D \frac{\dot{m}^3}{T_E \rho_E^2 A^3} L \left(1 + \frac{3\delta^*}{A} \right). \tag{4.18}$$

Thus the largest term in the expression for losses is the constant, so there is less dependence on boundary layer properties.

4.2 Effect of precompression zone characteristics

The effect of assumptions concerning the precompression zone is now examined. Figure 4-9 shows the power saving coefficient vs. ingested drag to airframe drag

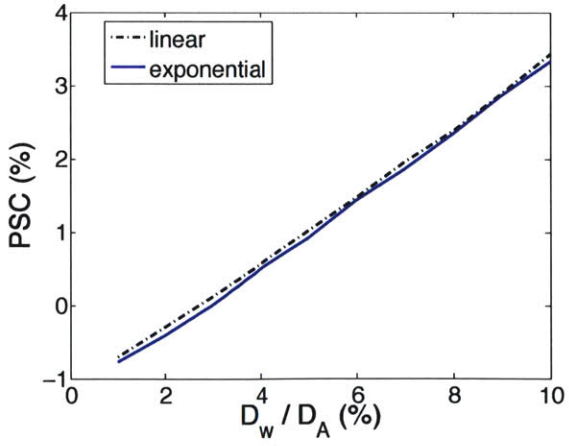

Figure 4-9: Comparison of the PSC for an exponential (blue plain line) and a linear (black dotted line) area variation in the precompression region

ratio for a linear and an exponential variation of the precompression zone area. The difference between the two curves is roughly 0.1%.

4.3 Effect of fan losses

The fan was assumed lossless so far. A non-ideal fan is now examined. The same efficiency and pressure ratio vs. corrected mass flow as for the parallel compressor model are chosen (Section 3.3). The power saving coefficient is shown in Figure 4-10 along with the results obtained for an ideal fan using the integral model. The figure shows more power is required with losses, because the operating point goes towards lower efficiencies, but the trend of the power saving coefficient remains the same. Figure 4-11 shows the difference between the power saving coefficient obtained with the compressible parallel model and the integral boundary layer description. Fan losses decrease the power saving coefficient, but don't change the trend of the power saving coefficient.

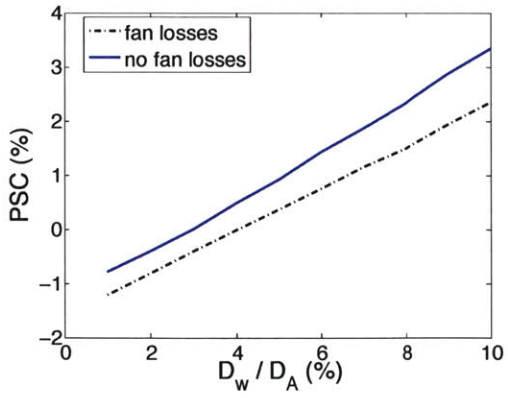

Figure 4-10: Power saving coefficient vs. ingested drag for ideal and non-ideal fans

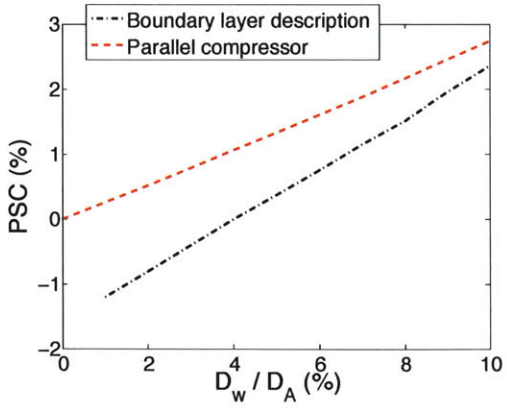

Figure 4-11: Power saving coefficient vs. ingested drag for a non-ideal fan using different models

4.4 Effect of fan - boundary layer interaction

The effect of the boundary layer change across the fan is now modeled parametrically. Figure 4-12 shows the effect of boundary layer ingestion assuming that the displacement and momentum thicknesses in the boundary layer at fan exit are related to those at fan inlet by a constant k,

$$[\delta^*, \theta]_d / A_d = k[\delta^*, \theta]_u / A_f, \tag{4.19}$$

with the shape factor, H, kept constant. The values of k have been varied from 0.5 to 2.

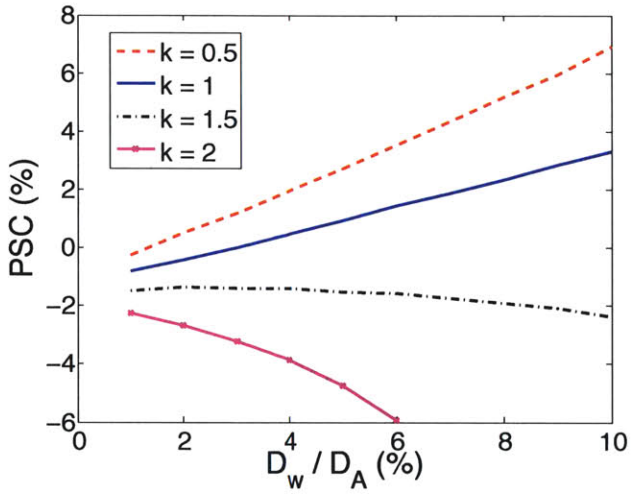

Figure 4-12: Sensitivity of the power saving coefficient to the change in *both* boundary layers across the fan: $[\delta^*, \theta]_d / A_d = k[\delta^*, \theta]_u / A_f$

The effect of boundary layer ingestion on the power saving coefficient changes from positive to negative as k varies. The physical reason for this is associated with the overall (duct average) blockage, which is larger as k increases so the pressure downstream of the fan drops. The fan thus has to put more work into the stream to get the required net thrust. Figures 4-13 and 4-14 give the effect of the "thin" boundary layer and the "thick" boundary layer change across the duct respectively, keeping the other boundary layer's thicknesses unchanged across the fan. The figures

show the contribution of the "thin" boundary layer is small and almost all of the difference in power saving coefficient is due to the "thick" boundary layer[8].

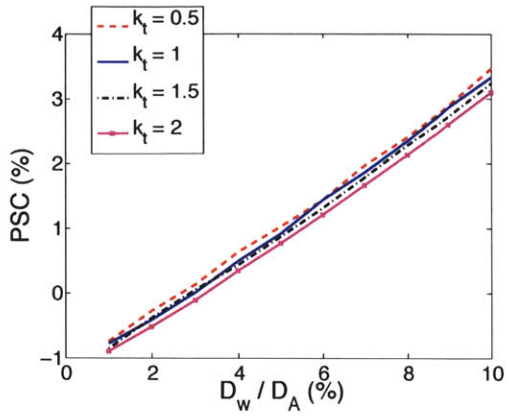

Figure 4-13: Sensitivity of the power saving coefficient to the change in "*thin*" boundary layer across the fan: $[\delta^*, \theta]_d/A_d = k_t[\delta^*, \theta]_u/A_f$

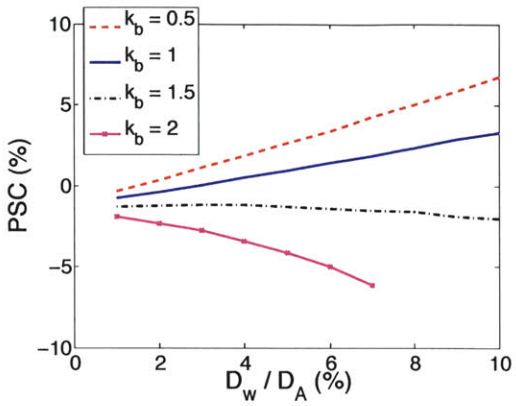

Figure 4-14: Sensitivity of the power saving coefficient to the change in "*thick*" boundary layer across the fan: $[\delta^*, \theta]_d/A_d = k_b[\delta^*, \theta]_u/A_f$

4.5 Conclusions on the integral boundary layer models

The integral model is useful for several reasons. First it shows the same trends for the power saving coefficient as the parallel compressor models. Second it demonstrates that inlet pressure recovery is not decreased with BLI, and, although the losses increase with BLI, they do not change the trend of the power saving coefficient. Third it shows the importance of the downstream blockage, e.g. the recovery factor, in setting the performance of the propulsion system with BLI. If the distortion is not attenuated enough across the fan, BLI is not beneficial.

[8]The calculations could not be carried out for high level of ingested drag and k equal to 1.5 or 2. The reason is that, in the case of $k > 1$, the mass flow increases with BLI and the prescribed inlet area is too small to pass all the flow

Based on these arguments, the key task appears to be to estimate the overall duct blockage for the essentially inviscid behavior of the fan and the "thick" boundary layer. The blockage is basically the distortion transfer across the fan. To address this for the type of distortions of interest (both circumferential and radial) a three-dimensional model is needed. These 3-D calculations are discussed in the next chapter.

Chapter 5

3-D fan distortion transfer calculations

Three-dimensional compressible calculations of the flow in a ducted fan are discussed in this chapter. The purpose is to include a higher fidelity calculation of the distortion transfer across the fan in the estimate of power saving coefficient as a function of boundary layer ingestion. The assumption is that the distortions of interest have length scales large to blade spacing and that the flow does not have to be resolved on the scale of a blade passage, so a body force analysis can be employed.

5.1 Computational model

The computational model used was developed by Gong [18] to compute the response of a multistage compressor to three-dimensional non-linear disturbances associated with instability and inlet distortions. The compression system is represented by a duct, blade rows, and a throttle. The flow in the duct is calculated by solving the 3-D unsteady inviscid Euler equations for mass, momentum and energy. For the flow in the blades the key idea is to model the effect of a blade row by a body force field. As mentioned above, the concept is to ignore the detailed flow structure in each individual blade passage, but to capture the flow redistribution between blade rows

and in each blade properly. The body force field reproduces the required pressure rise and flow turning and responds to steady and unsteady disturbances. The body forces are calculated from the blade inlet and exit metal angles and the flow local properties (more detail can be found in Gong [18]). Losses and deviation are added from a standard reference [27]. The exit condition is uniform static pressure downstream of the throttle.

The code requires the geometry of the duct and of the hub, the leading edge and trailing edge blade metal angles of the rotor and the stator, the number of blades, the rotational velocity, and a stagnation temperature and pressure profile at the entry of the computational domain.

5.2 Methodology for 3-D distortion transfer calculations

For the three-dimensional problem, a number of modeling questions must be addressed:

- what is an appropriate way to describe an inlet flow that goes from a semi-circular area to a circular area?
- what is the axial extent of the fan influence zone?
- how do we account for the hub geometry?
- does the core stream need to be modeled?
- how do we include the choked nozzle?
- how do we calculate the external expansion downstream of the nozzle?

5.2.1 Inlet flow

The first issue arises with modeling the inlet stagnation pressure profile. The S-duct area goes from semi-circular at the inlet to circular at the fan face. Gong's code only allows a circular duct area. The computational domain thus starts at a location

upstream of the fan where the duct is circular. For the region upstream of this, inlet calculations of Madani [30] for different levels of boundary layer ingestion are used. These calculations were done using a 3-D viscous CFD code and the inlet geometry is based on a NASA design. Hence the present calculations capture the duct curvature, the inlet losses, and the boundary layer change from the precompression zone to the circular fan face.

5.2.2 Fan

The region in which the upstream and downstream influence of the fan (upstream and downstream static pressure non-uniformity) exists is of the order of a diameter upstream and downstream. To be conservative a length two diameters upstream and downstream was chosen for the domain of the body force calculation.

5.2.3 Hub

Gong's code is based on a geometry with a hub. The radius of the hub was set at 0.08 of the casing radius upstream of the fan, the hub area is thus less than 1% of the fan face area.

5.2.4 Core stream

In the actual design, part of the flow is taken through the core engine between the rotor and the stator of the fan as sketched in Figure 5-1. It is not possible to represent the core stream in Gong's computation, and the hub is modeled as the streamline of the flow that splits the core and bypass streams.

5.2.5 Exhaust and jet expansion

The last issue concerns the flow downstream of the fan. The flow exits through a choked nozzle and expands to freestream static pressure downstream of the nozzle. The pressure becomes uniform at a location referred as the Trefftz Plane. The nozzle

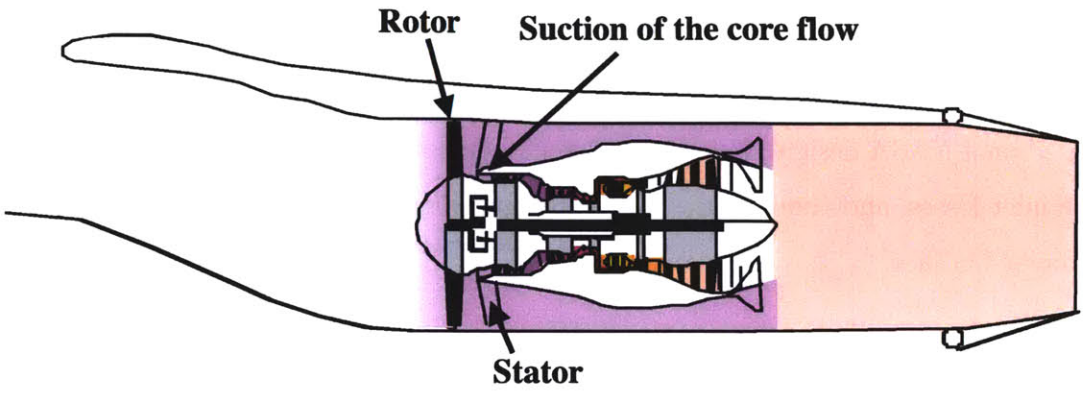

Figure 5-1: Engine schematic showing the suction of the core flow between the rotor and the stator, adapted from de la Rosa Blanco [7]

area is not known a priori for flow with inlet distortion, and the code does not capture external flow, but the momentum flux at the Trefftz Plane must be known to calculate the produced net thrust.

In the approach followed (see Figure 5-2), an ideal nozzle (no losses) is assumed in which "each streamtube expands independently without interaction with the rest of the flow down to atmospheric pressure" p_∞ [6]. With this assumption the net thrust is (Cumpsty and Horlock [6]):

$$T_N = \int \left(\sqrt{2c_p T_t \left[1 - \left(\frac{p_\infty}{p_t} \right)^{\frac{\gamma-1}{\gamma}} \right]} - u_\infty \right) \mathrm{d}\dot{m}. \tag{5.1}$$

5.2.6 Summary of the procedure [Refer to Figure 5-2]

The computational domain extends two fan diameters upstream and two fan diameters downstream of the fan to cover the zone of influence of the fan. It includes a hub. The core stream is neglected. The stagnation pressure profile at the entry of the domain comes from 3-D viscous calculations of the flow with inlet distortion in an S-duct. Duct, fan and hub designs were provided by Crichton [3][1].

[1]The fan design and inlet calculations are, in contrast to Chapters 3 and 4, for the second design of the Silent Aircraft's engine, GRANTA 3201

A 3-D inviscid calculation is done to estimate the flow in the computational domain using Gong's body force code. The net thrust is then calculated using equation (5.1). The fan power corresponding to this thrust is:

$$P = \int c_p (T_{t_d} - T_{t_u})\ \mathrm{d}\dot{m}. \tag{5.2}$$

This model is of higher fidelity than the parallel compressor and integral models, not only because it is based on three-dimensional calculations, but also because it now captures inlet losses and duct curvature.

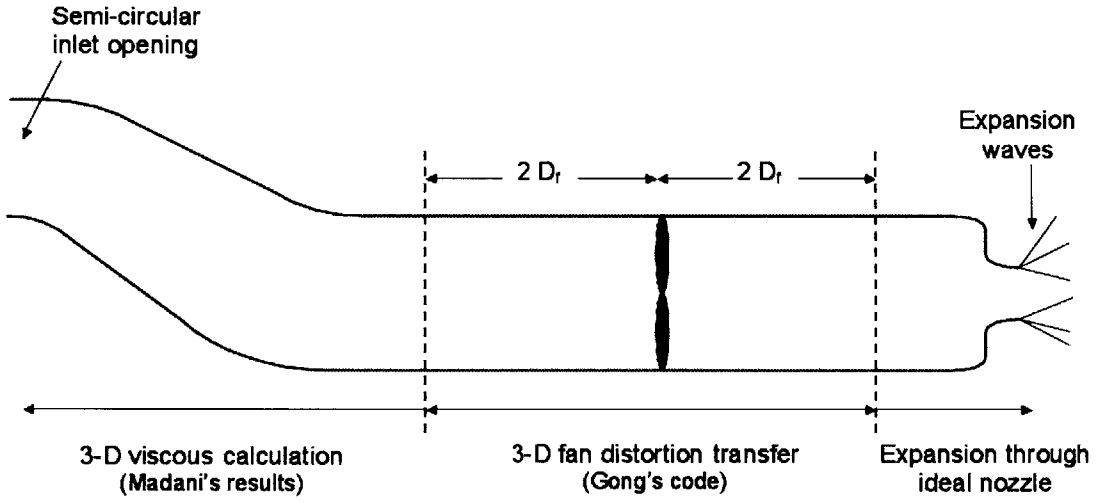

Figure 5-2: Sketch of the calculation procedure for the propulsion system

5.3 Discussion of the results

5.3.1 Fidelity of the model

The fidelity of the body force calculation was assessed by comparison with the 3-D results of Crichton [3]. Crichton designed a fan assuming a uniform incoming flow of stagnation pressure 0.96 times the freestream stagnation pressure (to account for

inlet losses and BLI). Calculations were carried out for the same conditions using the body force model with deviation and losses adjusted to obtain the same pressure ratio at the design point. The radial variation of the blade and flow exit angles from the rotor at design point is displayed in Figure 5-3[2].

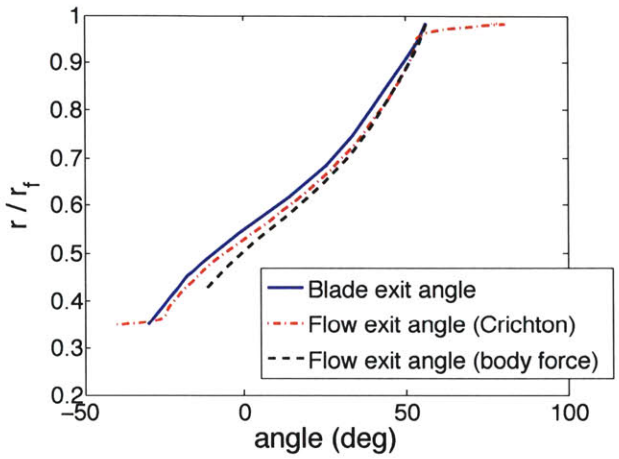

Figure 5-3: Comparison of blade and flow exit angles for body force analysis and for results of Crichton[3]

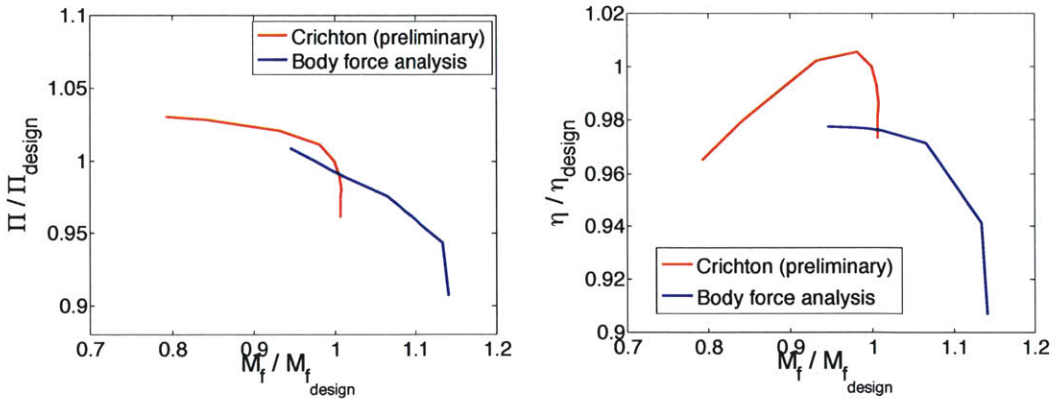

(a) Fan pressure ratio

(b) Efficiency

Figure 5-4: Fan characteristic for uniform flow vs. fan face Mach number[3]

[2]The blade metal angles are input in the body force approach so they are identical to those found by Crichton. The flow exit angle does not continue to the hub with the body force approach because the core stream is not modeled

It was not possible to match exactly the deviation at the hub and in the tip clearance. The pressure ratio vs. fan face Mach number is shown in Figure 5-4(a). The choking fan face Mach numbers are different by 13%. Based on one-dimensional flow, this corresponds to a difference of choking area of 6%. Since choking occurs in the rotor blades, and neither blade thickness nor boundary layers on the blades and the duct are modeled in the body force approach, this seems a reasonable difference attributable to blockage. The efficiency, shown in Figure 5-4(b), is lower than that obtained by Crichton because the body force analysis accounts for losses in the stator, whereas Crichton's calculations were for rotor only.

5.3.2 Fan characteristic for uniform flow

The thrust and fan power calculated using the body force approach is done first for a ducted fan with uniform incoming flow at freestream stagnation pressure as a baseline. The fan characteristic obtained and the design point are shown in Figure 5-5. The design point is set at the same fraction of fan face choking Mach number obtained by Crichton. The thrust and power, calculated using the method described in Section 5.2, will be used to define the power saving coefficient.

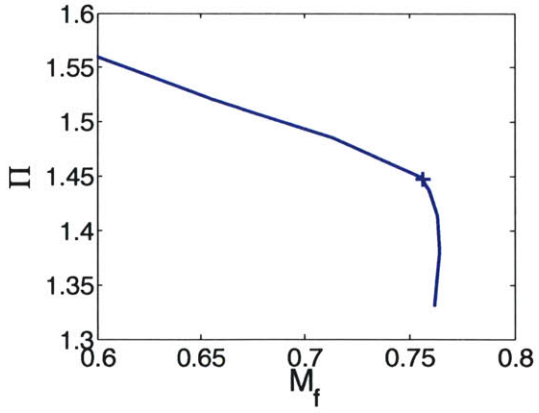

Figure 5-5: Fan characteristic for a ducted fan with uniform flow along with the design point
The x-axis is the fan face Mach number. The y-axis is the pressure ratio

[3]Crichton's results should be regarded as preliminary as the design is still evolving

5.3.3 Fan face distortion profiles

Five levels of boundary layer ingestion D_w/D_A were investigated, 4.5%, 9.0%, 14.8%, 20.2%, and 26.5%. Distortion profiles two diameters upstream of the fan for these different levels of BLI were provided by Madani [30], who carried out three-dimensional viscous calculations of the flow in a curved inlet for different boundary layer thickness to inlet height ratio δ/H.

The values of δ/H are given from the following considerations. The Mach number at the start of the precompression region is $M_0 = 0.92$ based on 3-D inviscid calculations over the airframe (Sargent [33]). A one-seventh power profile is assumed for the inlet boundary layer. The equation for ingested drag,

$$D_w = \rho u^2 \theta b \left(\frac{u}{u_\infty}\right)^{H_{avg}}, \tag{2.17}$$

gives θ. b is assumed to be one inlet diameter ($2H$). For a one-seventh power profile,

$$\frac{\delta^*}{\delta} = 0.125 \text{ and } \frac{\theta}{\delta} = 0.0972. \tag{5.3}$$

The levels of boundary layer ingestion examined thus correspond to boundary layer thickness to inlet height ratios of 10%, 20%, 33%, 45%, and 59%.

The distortion profile two diameters upstream of the fan for $D_w/D_A = 14.8\%$ is shown in Figure 5-6. This corresponds to the level of BLI expected for the current version of the Silent Aircraft. The region of low stagnation pressure presented to the fan varies both circumferentially and radially.

5.3.4 Power saving coefficient (PSC)

The power saving coefficient is shown in Figure 5-7. The power saving coefficient (PSC) is positive and increases with BLI. 2.9% power savings are obtained for 14.8% ingested drag. The calculated PSC does not go to zero when D_w/D_A goes to zero, because it goes to the ratio of the power required for a ducted fan with thin boundary

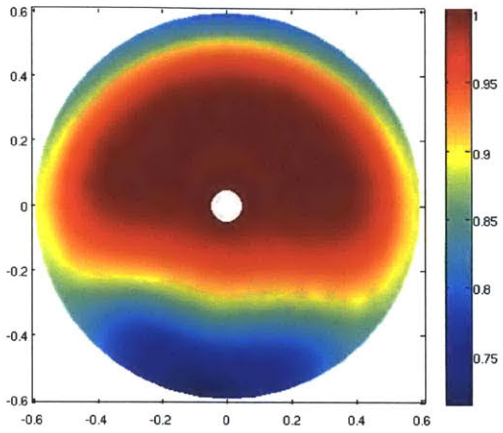

Figure 5-6: Stagnation pressure profile p_t/p_{t_∞} at two diameters upstream of the fan for 14.8% of ingested drag (calculation of Madani [30])

layers in an S-duct (embedded engine without BLI) to the power required for uniform flow in a straight lossless duct (podded engine without BLI and without losses)[4]. This ratio is negative. To account for losses in the podded case, a simple one-dimensional estimate of the difference in power due to (thin) boundary layers in a podded engine was carried out. This amounts to a comparison between the power for uniform flow, and an integral boundary layer calculation of the power for uniform flow with thin boundary layers. The power saving coefficient corrected using these two values is shown as the red dashed line in Figure 5-7. The corrected estimate for the power saving coefficient for 14.8% ingested drag is 3.8%.

The estimates of the parallel compressor and integral boundary layer approaches give a PSC with the same trend as the 3-D calculations, although the former are more optimistic.

The changes in fan characteristic (pressure ratio vs. fan face mass average Mach number) and operating point are shown in Figure 5-8. The curves collapse for different levels of BLI.

[4]This is because the baseline for the power saving coefficient is uniform inviscid flow at freestream stagnation pressure in a ducted fan as described in Section 5.3.2

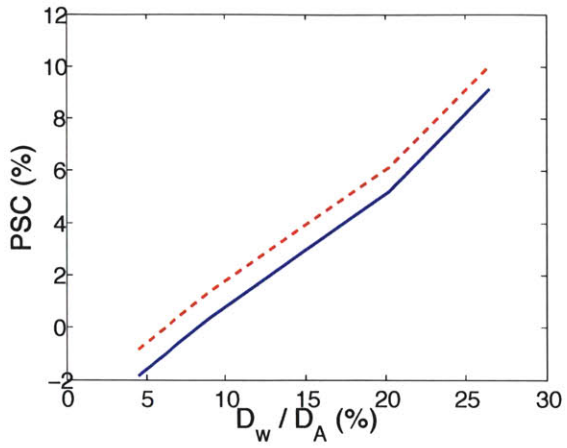

Figure 5-7: Power saving coefficient vs. ratio of ingested drag to airframe drag The baseline for the blue plain line is podded engines without duct losses. The baseline for the red dashed line is podded engines with duct losses

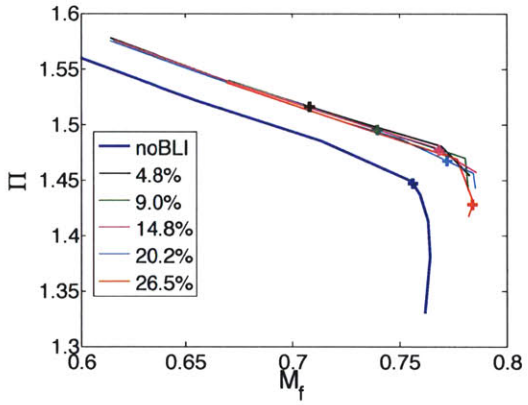

Figure 5-8: Fan characteristic for different levels of boundary layer ingestion The x-axis is the fan face mass average Mach number. The y-axis is the fan pressure ratio

5.3.5 Distortion transfer across the fan

Figures 5-9(a) and 5-9(b) show the stagnation pressure profile at the exit of the fan and at two diameters downstream of the fan. The inlet distortion is that of Figure 5-6. The downstream region of low stagnation pressure does not correspond in a

simple manner to that seen upstream. A description in terms of a boundary layer and a uniform stream (as in Chapter 4) is thus not appropriate for the flow structure.

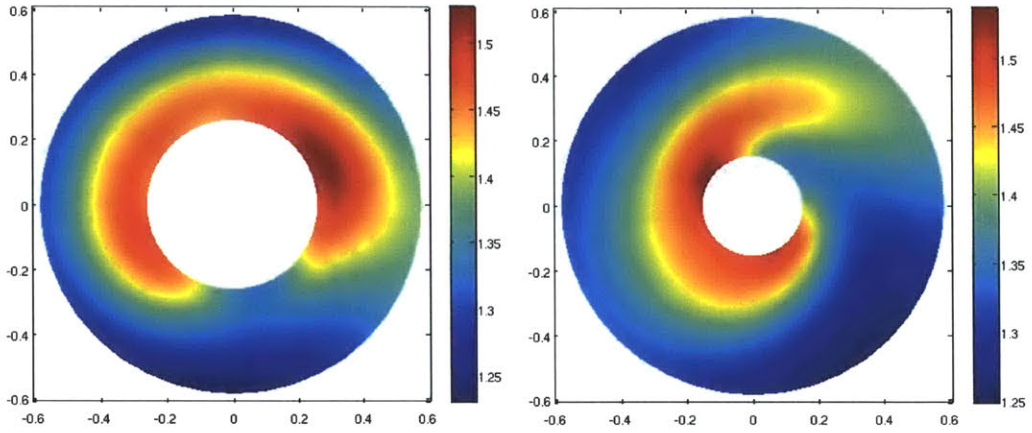

(a) At the fan exit

(b) Two diameters downstream

Figure 5-9: Stagnation pressure profiles p_t/p_{t_∞} for 14.8% of ingested drag

5.3.6 Static pressure

The static pressure at the fan exit is shown in Figure 5-10(b). It is not uniform as was assumed in the parallel compressor model (Chapter 3). The static pressure is not uniform at the fan face, as can be seen in Figure 5-10(a).

5.4 Conclusions on the 3-D calculations

Three-dimensional calculations of the inviscid flow in a ducted fan with inlet distortion were carried out using a body force model. They show the approximations done for the parallel compressor and integral models are not valid in terms of flow structure. The flow downstream of the fan does not correspond to a boundary layer and an inviscid stream, and the static pressure is not uniform across the duct. However, the 3-D calculations demonstrate the same trend for the power saving coefficient, and

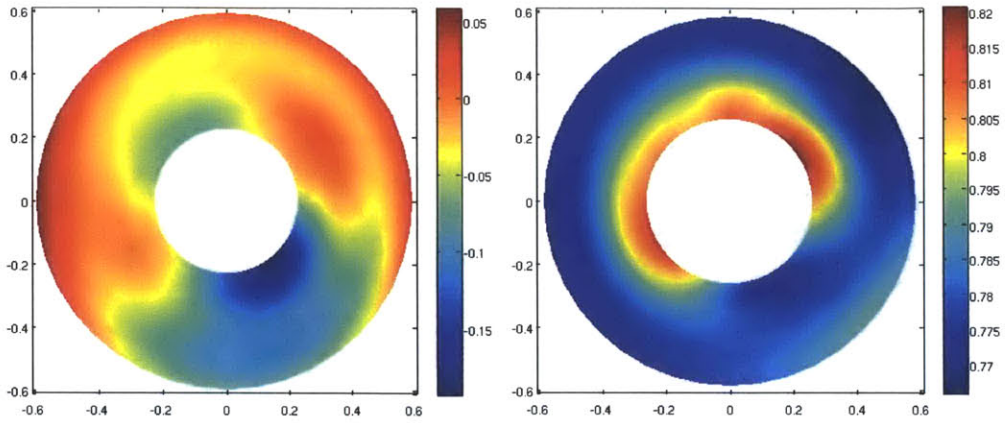

(a) At the fan face

(b) At the fan exit

Figure 5-10: Static pressure profiles $(p - p_\infty) / 0.5\rho_\infty U^2$ for 14.8% of ingested drag U is the fan tip speed.

show that several percent power savings are achievable provided enough boundary layer is ingested.

Chapter 6

Conclusions

6.1 Summary and conclusions

1. This thesis provides a first-of-a-kind assessment of the aerodynamic performance of a propulsion system with boundary layer ingestion (BLI) including a description of turbomachinery (i.e., fan) operation in non-uniform flow. The figure of merit for the embedded engine configuration investigated was the power saving coefficient (the difference between required fan power as a function of the amount of boundary layer ingested) for a given airframe drag, fan diameter, and flight conditions.

2. To examine the modeling requirements for the propulsion systems of interest, the assessment also included comparison of models of three different degrees of fidelity: a one-dimensional parallel compressor approach, an integral boundary layer type of analysis, and a fully three-dimensional body force model of the non-uniform flow into the fan. The last of these is able to capture the fan response to the type of combined circumferential and radial distortion typically associated with BLI and to provide insight into the flow field structure resulting from the distortion.

3. For the estimated level of BLI in an aircraft design under consideration for the Silent Aircraft Initiative, the most detailed calculations carried out gave a power

saving between 3 and 4%.

4. For the types of boundary layer ingestion investigated the principal feature required to estimate the power saving was found to be the distortion transfer across the fan, i.e. the (largely inviscid) attenuation of the non-uniform stagnation pressure presented to the fan. The level of non-uniformity in the duct downstream of the fan is a major aspect of determining the necessary fan pressure rise and the thrust, and thus fan power needed.

5. The quantitative results for power saving coefficient differed by 10-40% between the different models. However all the approaches gave the same qualitative trends, namely that several percent in fuel burn was provided by the use of BLI.

6. With embedded engines, in contrast to podded engines without boundary layer ingestion, calculations of thrust and drag involve the characteristics of both the engine and the airframe. New definitions of thrust and drag were thus developed to account for the highly integrated configurations of airframes and propulsion systems of interest.

6.2 Future work

Possible future work includes investigating the sensitivity of the power saving coefficient to the changes in design parameters such as fan area, fan characteristic (and fan rotational speed), flight velocity, and velocity and boundary layer properties at the start of the precompression zone. 3-D distortion transfer calculations should also be done with blade thicknesses and blockage in the rotor. Another possible enhancement of the 3-D model is to include the core stream to assess in more detail the effect of BLI on the core thermal efficiency. Finally, although not adressed in this thesis, the impact of distortion on fan operability, aeromechanical response, and noise should be assessed.

Appendix A

A treatment of BLI in terms of energy and propulsive efficiency

The origin of the benefits due to boundary layer ingestion is usefully described from the ground reference frame, following Douglass [9][1]. The unsteadiness of the flow in the ground reference frame precludes the use of the steady flow energy equation, and the first law of thermodynamics is thus applied to a unit mass, as explained in Küchemann [25]. If the mass goes from state 1 to state 2, its change in total energy must be equal to the heat received minus the shaft work done minus the work done by the movement of the system on the surroundings (the $p\mathrm{d}V$ work). The work per unit mass done by the flow on the constant pressure surroundings is,

$$w = \frac{p}{\rho}. \tag{A.1}$$

The first law is thus written:

$$\Delta\left(e + \frac{u^2}{2} + \frac{p}{\rho}\right) = q - w_{shaft}, \tag{A.2}$$

where q is the heat per unit mass received by the flow, and w_{shaft} the work done by the flow on its surroundings other than pressure work. Equation A.2 can be written

[1]The induced drag will be neglected for this analysis

as:

$$\Delta\left(c_pT + \frac{u^2}{2}\right) = q - w_{shaft}. \tag{A.3}$$

A.1 Conservation of energy for podded engines

For an aircraft with podded engines, the energy given by the engine to the flow must be seen downstream of the aircraft. The flow far downstream consists of two parts: the wake due to the airframe and the jet due to the engine. Consider a unit mass m of air that is intially at rest (state 1), goes around the airframe, and forms the wake downstream of the airframe when returned at freestream static pressure (state 2). The first law can be applied to to this mass from state 1 to state 2 with heat transfer neglected. The change in stagnation enthalpy is,

$$\Delta h_{t_{wake}} = \Delta\left(c_pT + \frac{u^2}{2}\right) = \left(c_p(T_w - T_\infty) + \frac{(u_\infty - u_w)^2}{2}\right). \tag{A.4}$$

In equation (A.4) T_w and u_w are the static temperature and relative velocity (velocity in the aircraft reference frame) in the wake. Equation (A.2) shows this change in stagnation enthalpy is the energy per unit mass given to the flow denoted as E_{wake}. The energy in the wake consists of two parts, the kinetic energy of the wake, and the so-called "enthalpy wake" (Douglass [9]). T_w can be found by considering the steady flow energy equation in the aircraft frame of reference. In that frame the stagnation temperature in the airframe wake can be considered as constant and equal to the freestream stagnation temperature. Thus,

$$T_{t_\infty, aircraft} = T_\infty + \frac{u_\infty^2}{2c_p} = T_{t_w, aircraft} = T_w + \frac{u_w^2}{2c_p}. \tag{A.5}$$

Combining equations (A.4) and (A.5) yields:

$$E_{wake} = \frac{(u_\infty - u_w)^2}{2} + \left(\frac{u_\infty^2}{2} - \frac{u_w^2}{2}\right). \tag{A.6}$$

Rearranging equation (A.6) gives the energy per unit mass required for flight to sustain the airframe drag per unit mass D_A,

$$E_{wake} = (u_\infty - u_w)u_\infty = D_A u_\infty = (u_j - u_\infty)\, u_\infty = E_{useful}. \tag{A.7}$$

The first law is now applied to a unit mass m that goes through the engine from rest to downstream of the aircraft when returned at freestream static pressure. The change in stagnation enthalpy per unit mass of the flow is,

$$\Delta h_{t_{jet}} = c_p(T_j - T_\infty) + \frac{(u_j - u_\infty)^2}{2}, \tag{A.8}$$

where u_j is the relative jet velocity (velocity in the aircraft reference frame) and T_j is the static temperature in the jet. The change in stagnation enthalpy of the flow is equal to the energy given by the aircraft to the jet E_{jet}.

The total energy per unit mass added to the flow, as seen in the ground fixed system, is thus:

$$\begin{aligned}
E_{added} &= E_{wake} + E_{jet}, && \text{(A.9)}\\
&= D_A u_\infty + \frac{(u_j - u_\infty)^2}{2} + c_p(T_j - T_\infty), && \text{(A.10)}\\
&= (u_j - u_\infty)u_\infty + \frac{(u_j - u_\infty)^2}{2} + c_p(T_j - T_\infty), && \text{(A.11)}\\
&= \frac{u_j^2 - u_\infty^2}{2} + c_p(T_j - T_\infty). && \text{(A.12)}
\end{aligned}$$

Equation (A.12) describes the energy produced by the engine as seen in the moving frame of reference. The first term is available mechanical energy while the second term (heat) is, in this situation, non-recoverable energy.

The lost energy per unit mass (energy not used in propelling the fluid) is equal to

the added energy minus the useful energy:

$$E_{lost} = E_{added} - E_{useful} = E_{wake} + E_{jet} - E_{useful} = E_{jet} = \frac{(u_j - u_\infty)^2}{2} + c_p(T_j - T_\infty). \tag{A.13}$$

The lost energy is therefore the kinetic energy left in the jet plus the enthalpy wake energy. The latter is not recoverable but the kinetic energy is still available to the system.

Propulsive efficiency

The author has been unable to find a universally accepted definition of the propulsive efficiency. Three different definitions are given here for comparison. Table A.1 summarizes the notations of the three authors. Küchemann [25] defines the overall propulsive efficiency as the ratio of the propulsive work per unit weight to the energy input per unit weight:

$$\eta = \frac{Tu_\infty}{\bar{q} + \bar{w}}. \tag{A.14}$$

In equation (A.14) T is the propulsive force per unit weight, $\bar{q}$ is the heat received per unit weight, and $\bar{w}$ is the work done per unit weight. This efficiency is the product of the mechanical jet efficiency, defined as the ratio of the propulsive work to the added kinetic energy per unit weight Δe_k,

$$\eta_j = \frac{Tu_\infty}{\Delta e_k}, \tag{A.15}$$

and of the kinetic efficiency,

$$\eta_k = \frac{\Delta e_k}{\bar{q} + \bar{w}}. \tag{A.16}$$

Smith [36] defines the propulsive power as the increase in axial kinetic energy times the mass flow:

$$P_p = \dot{m}_e \left(\frac{u_j^2}{2} - \frac{u_\infty^2}{2} \right). \tag{A.17}$$

Smith's propulsive efficiency is:

$$\eta_p = \frac{u_\infty T}{P_p}. \tag{A.18}$$

He also defines an efficiency relating the propulsive power P_p to the actual shaft power P:

$$\eta_{KE} = \frac{P_p}{P}. \tag{A.19}$$

He finally defines an overall propulsor efficiency as:

$$\eta = \frac{u_\infty T}{P} = \eta_p \eta_{KE}. \tag{A.20}$$

Cumpsty [5] defines the propulsive efficiency as the ratio of the thrust power to the power to the jet,

$$\eta_p = \frac{u_\infty T_N}{\dot{m}_e \Delta KE} = \frac{u_\infty T_N}{\frac{1}{2}\dot{m}_e (u_j - u_\infty)}, \tag{A.21}$$

where T_N is the net thrust, $\dot{m}_e$ is the engine mas flow and ΔKE is the increase in axial kinetic energy of the jet. He defines the thermal efficiency as the ratio of the power to jet to the thermal power from fuel:

$$\eta_{th} = \frac{\dot{m} \Delta KE}{\dot{m}_f LCV}. \tag{A.22}$$

In equation (A.22) $\dot{m}_f$ is the fuel mass flow and LCV is the low calorific value of fuel. The overall efficiency is defined by Cumpsty as the product of the thermal and propulsive efficiencies,

$$\eta = \eta_{th} \eta_p. \tag{A.23}$$

In this thesis, the propulsive efficiency is defined as the ratio of thrust power to mechanical power, or power available, and is, in the case of podded engines, the well-known Froude efficiency (Küchemann [25]):

$$\eta_p = \frac{P_{useful}}{\dot{m}_e KE_{added}} = \frac{P_{useful}}{\frac{\dot{m}_e}{2}(u_j^2 - u_\infty^2)} = \frac{2u_\infty}{u_\infty + u_j}. \tag{A.24}$$

The propulsive efficiency in equation (A.24) measures how efficient the aircraft is in converting available power ($\dot{m}_e KE_{added}$) into useful power ($D_A u_\infty$). It is a measure of the lost available energy, e.g. the kinetic energy left in the jet per unit time:

$$1 - \eta_p = \frac{\dot{m}_e \frac{(u_j - u_\infty)^2}{2}}{\dot{m}_e KE_{added}}. \tag{A.25}$$

The overall efficiency is defined as:

$$\eta = \frac{P_{useful}}{P_{added}}. \tag{A.26}$$

In the case of a ducted fan, the added power P_{added} is the power absorbed by the fan, so the overall efficiency defined as in equation (A.26) is similar to Smith's definition of the overall propulsor efficiency.

A.2 Conservation of energy for embedded engines with BLI

Consider now that 100% of the boundary layer is ingested. Following the same method as for podded engines (equations (A.4)-(A.7)), the energy per unit mass added to the flow to go from rest (state 1) to the wake at freestream static pressure (state 2) is:

$$E_{wake} = \frac{(u_\infty - u_w)^2}{2} + \left(\frac{u_\infty^2}{2} - \frac{u_w^2}{2}\right) = (u_\infty - u_w)u_\infty = E_{useful}. \tag{A.27}$$

Then the energy per unit mass added by the engine to this mass from wake (state 2) to jet (state 3) is:

$$E_{engine} = c_p T_j + \frac{(u_j - u_\infty)^2}{2} - c_p T_w - \frac{(u_\infty - u_w)^2}{2}. \tag{A.28}$$

There is no kinetic energy left in the jet, so $u_j = u_\infty$. Using equation (A.5) yields,

$$E_{engine} = c_p(T_j - T_\infty) - (u_\infty - u_w)u_\infty. \tag{A.29}$$

Rearranging equation (A.28) gives,

$$E_{engine} = c_p(T_j - T_w) - \frac{(u_\infty - u_w)^2}{2}. \tag{A.30}$$

The first term is the energy given by the engine (positive term). The second term is the kinetic energy of the wake used by the engine to provide thrust (negative term). Combining equations (A.28) and (A.27), the energy added to a unit mass by the aircraft from rest to downstream of the aircraft at freestream static pressure is:

$$E_{added} = c_p(T_j - T_\infty) = c_p(T_j - T_w) + \left(\frac{u_\infty^2}{2} - \frac{u_w^2}{2}\right). \tag{A.31}$$

The energy added to the flow is the "enthalpy wake" energy left behind the aircraft. The second expression for the added energy is exactly the energy added by the engine to the flow from the aircraft frame of reference. The difference between the added energy and the useful energy is therefore:

$$E_{added} - E_{useful} = c_p(T_j - T_w) - \frac{(u_\infty - u_w)^2}{2}. \tag{A.32}$$

Boundary layer ingestion is beneficial because the engine uses the kinetic energy of the wake. Another way of stating this is that BLI reduces the kinetic energy left in the jet.

Propulsive efficiency

Using the same definition as for podded engines, the propulsive efficiency is,

$$\eta_p = \frac{P_{useful}}{\dot{m}_e K E_{added}} = \frac{\dot{m}_e(u_\infty - u_w)u_\infty}{\dot{m}_e\left(\frac{u_\infty^2}{2} - \frac{u_w^2}{2}\right)} = \frac{2u_\infty}{u_\infty + u_w}. \tag{A.33}$$

Equation (A.33) shows η_p is always greater than 1 and the maximum attainable value is 2, because some of the useful work is used to provide thrust.

The overall efficiency is defined as in equation (A.26).

Table A.1: Summary of the different definitions of propulsive efficiencies

Küchemann			
Input	Work and heat		
	$\bar{q} + \bar{w}$		
	$\Downarrow$	Kinetic efficiency η_k	
	Mechanical energy		Overall propulsive efficiency
	Δe_k		$\eta_p = \eta_j \eta_k$
	$\Downarrow$	Jet efficiency η_j	
Useful E	Propulsive work		
	Tu_∞		
Smith			
Input	Shaft power		
	P		
	$\Downarrow$	Kinetic efficiency η_{KE}	
	Propulsive power		Overall propulsor efficiency
	$P_p = \dot{m}_e \Delta KE$		$\eta = \eta_p \eta_{KE}$
	$\Downarrow$	Propulsive efficiency η_p	
Useful P	Thrust power		
	$u_\infty T$		
Cumpsty			
Input	Thermal energy		
	$\dot{m}_f LCV$		
	$\Downarrow$	Thermal efficiency η_{th}	
	Power to jet		Overall efficiency
	$\dot{m}_e \Delta KE$		$\eta = \eta_p \eta_{th}$
	$\Downarrow$	Propulsive efficiency η_p	
Useful P	Thrust power		
	$u_\infty T_N$		

Appendix B

Coles profile

A useful description of a turbulent boundary layer is the "Coles" profile [13]. The velocity u in a two-dimensional boundary layer is given as a function of the height in the duct y, the velocity at the edge of the boundary layer u_E, the boundary layer thickness δ and a non-dimensional parameter U_s. The relation between u and y is:

$$\frac{u}{u_E} = U_s + (1 - U_s)\left[\frac{1}{2} - \frac{1}{2}\cos\left(\pi\frac{y}{\delta}\right)\right]. \tag{B.1}$$

The actual profile and the Coles profile are sketched in Figure B-1. The upper part of

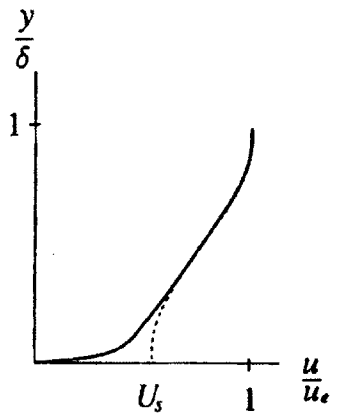

Figure B-1: Coles profile (dotted line) and actual profile (plain line) for a turbulent boundary layer, taken from Drela [13]

the boundary layer is well matched. The lower part is not and the no-slip condition is

not captured. The assumption in using this is that it is more important to match the upper parts of the boundary layers. This is certainly reasonable since the lower part of the boundary layer does not contribute much to the momentum and the kinetic energy of the boundary layer, which scale as u^2 and u^3 respectively.

From the Coles profile, the boundary layer displacement thickness is then:

$$\frac{\delta^*}{\delta} = \frac{1 - U_s}{2}. \tag{B.2}$$

The momentum thickness is:

$$\frac{\theta}{\delta} = \frac{1 - U_s}{2} - \frac{3}{8}(1 - U_s)^2. \tag{B.3}$$

The shape factor is:

$$\frac{H - 1}{H} = \frac{3}{4}(1 - U_s). \tag{B.4}$$

The Coles profile is used when the boundary layer integral thicknesses δ^* and θ are known and an actual boundary layer is needed, for example to calculate an average stagnation pressure. In that case, U_s and δ are calculated from Equations (B.2) and (B.3).

Appendix C

Integral boundary layer equations

Solving the integral boundary layer equations allows to calculate the interaction of the boundary layer and the core flow in a quasi one-dimensional duct. These equations are derived here following Drela [13]. The nomenclature used is shown in Figure C-1. The momentum thickness θ_0, the displacement thickness δ_0^* and the inviscid velocity u_0 are given at the inlet of the duct, the area $A(x)$ and the length L of the duct are also specified. The stagnation temperature and pressure are considered constant in the inviscid part of the flow. The static pressure is assumed constant across the duct. u_E denotes the velocity at the edge of the boundary layer throughout Appendix C.

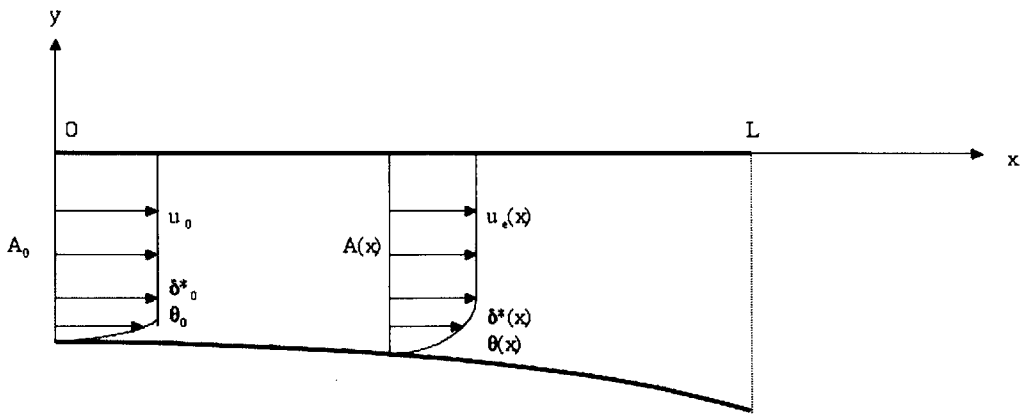

Figure C-1: Nomenclature for the integral boundary layer equations for a duct of length L and area $A(x)$

C.1 Derivation of the equations

Equations for the boundary layer

The first two equations of the system come from the continuity and conservation of momentum for the boundary layer. The core stream is assumed inviscid. Thus the momentum equation for the core stream is:

$$u_E \frac{\mathrm{d}u_E}{\mathrm{d}x} = -\frac{1}{\rho_E}\frac{\mathrm{d}p_E}{\mathrm{d}x}. \tag{C.1}$$

The conservation of mass and momentum for the boundary layer are:

$$\frac{\partial \rho u}{\partial x} + \frac{\partial \rho v}{\partial y} = 0, \tag{C.2}$$

$$\rho u \frac{\partial u}{\partial x} + \rho v \frac{\partial u}{\partial y} - \rho_E u_E \frac{du_E}{dx} - \frac{\partial \tau}{\partial y} = 0. \tag{C.3}$$

Integrating across the equations across the boundary layer as explained below gives the system of equations (C.4)-(C.5).

$$\int_0^\delta [(u-u_E)\times(C.2)+(C.3)]\,\mathrm{d}y \quad \Rightarrow \quad \frac{\mathrm{d}}{\mathrm{d}x}\left(\rho_E u_E^2 \theta\right) = \tau_w - \rho_E u_E \delta^* \frac{\mathrm{d}u_E}{\mathrm{d}x}, \tag{C.4}$$

$$\int_0^\delta \left[(u^2-u_E^2)\times(C.2)+2u\times(C.3)\right]\,\mathrm{d}y \quad \Rightarrow \quad \frac{\mathrm{d}}{\mathrm{d}x}\left(\rho_E u_E^3 \theta^*\right) = 2D - 2\rho_E u_E^2 \delta_e^{**} \frac{\mathrm{d}u_E}{\mathrm{d}x}. \tag{C.5}$$

In a dimensionless form, this system is:

$$\frac{\mathrm{d}\theta}{\mathrm{d}x} = \frac{C_f}{2} - (H+2-M_E^2)\frac{\theta}{u_E}\frac{\mathrm{d}u_E}{\mathrm{d}x}, \tag{C.6}$$

$$\frac{\mathrm{d}\theta^*}{\mathrm{d}x} = 2C_D - \left(\frac{2H^{**}}{H^*}+3-M_E^2\right)\frac{\theta^*}{u_E}\frac{\mathrm{d}u_E}{\mathrm{d}x}. \tag{C.7}$$

Equation (C.6) is the Von-Karman intergral momentum equation. Equation (C.7) is the integral kinetic energy equation. Equation (C.7) can be replaced by the following equation by $\frac{1}{H^*}(C.7) - (C.6)$:

$$\frac{\theta}{H^*}\frac{\mathrm{d}H^*}{\mathrm{d}x} = \frac{2C_D}{H^*} - \frac{C_f}{2} + \left(H - 1 - \frac{2H^{**}}{H^*}\right)\frac{\theta}{u_E}\frac{\mathrm{d}u_E}{\mathrm{d}x}. \tag{C.8}$$

Equation for the freestream

The global continuity equation for the duct is:

$$\rho_E u_E = \frac{\dot{m}}{\rho(A - \delta^*)}. \tag{C.9}$$

Differentiating equation (C.9) with respect to x leads:

$$\frac{\mathrm{d}u_E}{\mathrm{d}x} = \frac{u_E}{A - \delta^*}\left(\frac{\mathrm{d}\delta^*}{\mathrm{d}x} - \frac{\mathrm{d}A}{\mathrm{d}x}\right)\frac{1}{1 - M_E^2}. \tag{C.10}$$

System of equations

The system of integral boundary layer equations is thus:

$$\frac{\mathrm{d}\theta}{\mathrm{d}x} = \frac{C_f}{2} - (H + 2 - M_E^2)\frac{\theta}{u_E}\frac{\mathrm{d}u_E}{\mathrm{d}x}, \tag{C.11}$$

$$\frac{\theta}{H^*}\frac{\mathrm{d}H^*}{\mathrm{d}x} = \frac{2C_D}{H^*} - \frac{C_f}{2} + \left(H - 1 - \frac{2H^{**}}{H^*}\right)\frac{\theta}{u_E}\frac{\mathrm{d}u_E}{\mathrm{d}x}, \tag{C.12}$$

$$\frac{\mathrm{d}u_E}{\mathrm{d}x} = \frac{u_E}{A - \delta^*}\left(\frac{\mathrm{d}\delta^*}{\mathrm{d}x} - \frac{dA}{dx}\right)\frac{1}{1 - M_E^2}. \tag{C.13}$$

C_f, C_D, H^* and H^{**} are functions of M_E, H and the momentum thickness Reynolds number Re_θ. These functions can be found empirically through turbulent closure as explained in Appendix D. Thus the only unknown of the system is the vector $\mathbf{X} = [\theta\ \delta^*\ u_E]^t$. Given the initial conditions at $x_0 = 0$, the flow can be known for $0 \leq x \leq L$.

C.2 Solution procedure: Newton's method

This ODE system of equations (C.11)-(C.13) can be solved using Newton's method. The x-space is divided into N+1 points $(x_k)_{0\leq k\leq N}$ such that the grid step is: $dx = L/N$. At station $x_0 = 0$, $\mathbf{X}_0 = [\theta_0 \ \delta_0^* \ u_0]^t$ is known.

At each streamwise location x_k, H_k, M_k, $Re_k = \dfrac{\rho_k u_k \theta_k}{\mu}$, H_k^*, H_k^{**}, C_{f_k}, C_{D_k} and there derivatives with respect to $\mathbf{X}_k$ can be calculated. To calculate $\mathbf{X}_{k+1}$, the residual of the system $\mathbf{R}$ must be zero:

$$\mathbf{R}\left(\mathbf{X}_k, \mathbf{X}_{k+1}\right) = 0. \tag{C.14}$$

Newton's method is used to solve this equation. This method is based on a first order Taylor development of the equation. To first order,

$$\mathbf{R}\left(\mathbf{X}_k, \mathbf{y} + \delta\mathbf{y}\right) = \mathbf{R}\left(\mathbf{X}_k, \mathbf{y}\right) + \frac{\partial}{\partial \mathbf{y}}\mathbf{R}\left(\mathbf{X}_k, \mathbf{y}\right)\delta\mathbf{y}. \tag{C.15}$$

A series X_{k+1}^n can be created in the following way:

$$\mathbf{X}_{k+1}^{n+1} = \mathbf{X}_{k+1}^n + \delta\mathbf{X}^n, \tag{C.16}$$

$$\delta\mathbf{X}^n = -\left(\frac{\partial \mathbf{R}^n}{\partial \mathbf{X}_{k+1}^n}\right)^{-1}\mathbf{R}^n, \tag{C.17}$$

where $\mathbf{R}^n = \mathbf{R}\left(\mathbf{X}_k, \mathbf{X}_{k+1}^n\right)$. This series will converge quadratically towards $\mathbf{X}_{k+1}$. Newton algorithm is stopped when the Newton step is less than $\epsilon = 10^{-11}$.

Appendix D

Turbulent boundary layer coefficients

The coefficients for a compressible turbulent boundary layer were taken from Drela [11]. They are assumed to be only dependent on the kinematic shape factor H_k (defined below in equation D.2), the edge Mach number M_E, and the momentum thickness Reynolds number Re_θ defined as:

$$Re_\theta = \frac{\rho_E u_E \theta}{\mu_E}. \tag{D.1}$$

H_k is the kinematic shape factor, "which is defined with the density across the boundary layer assumed constant" [11].

$$H_k = \frac{H - 0.290 M_E^2}{1 + 0.113 M_E^2}. \tag{D.2}$$

The **skin friction coefficient** C_f is defined as:

$$C_f = \frac{\tau_w}{\frac{1}{2}\rho_E u_E^2}, \tag{D.3}$$

where τ_w is the wall shear stress, ρ_E and u_E are the edge density and velocity. C_f is

derived from Swafford,

$$F_C C_f = \frac{0.3e^{-1.33H_k}}{\left[\log_{10}\left(\frac{Re_\theta}{F_C}\right)\right]^{1.74+0.31H_k}} + 1.1\times 10^4 \left[\tanh\left(4-\frac{H_k}{0.875}\right)-1\right]. \tag{D.4}$$

In equation (D.4),

$$F_C = \sqrt{1+0.2M_E^2}. \tag{D.5}$$

The **dissipation coefficient** C_D is defined as:

$$C_D = \frac{D}{\rho_E u_E^3} = \frac{1}{\rho_E u_E^3}\int_0^\delta \tau \frac{\partial u}{\partial y} dy, \tag{D.6}$$

and is derived from G-β locus, assuming equilibrium flow,

$$\frac{2C_D}{H^*} = 0.5C_f\left(\frac{4}{H_k}-1\right)\frac{1}{3} + 0.03\left(1-\frac{1}{H_k}\right)^3. \tag{D.7}$$

The **energy factor** was derived by Drela from log-law and Coles turbulent profile. He first defined H_0 as follows:

$$\begin{aligned} H_0 &= 3+\frac{400}{Re_\theta} && \text{if } Re_\theta > 400, \\ &= 4 && \text{else.} \end{aligned} \tag{D.8}$$

The kinematic energy factor is then:

$$\begin{aligned} H_k^* &= \left(2-1.5-\frac{4}{Re_\theta}\right)\left(\frac{H_0-H_k}{H_0-1}\right)^2 \frac{1.5}{H_k+0.5} + 1.5 + \frac{4}{Re_\theta} && \text{if } H_k < H_0, \\ &= (H_k-H_0)^2\left(0.007\frac{\log Re_\theta}{\left(H_k-H_0+\frac{4}{\log Re_\theta}\right)^2}+\frac{0.055}{H_k}\right)+1.5+\frac{4}{Re_\theta} && \text{else.} \end{aligned} \tag{D.9}$$

The energy factor is:

$$H^* = \frac{H_k^* + 0.028M_E^2}{1.0+0.014M_E^2}. \tag{D.10}$$

The **density thickness** factor is:

$$H^{**} = \left(\frac{0.064}{H_k - 0.8} + 0.251 \right) M_E^2. \tag{D.11}$$

Bibliography

[1] A. Betz, *Introduction to the Theory of Flow Machines.* Pergamon Press, 1966, chapter 59, pp. 215–220.

[2] R. L. Campbell, M. B. Carter, and O. C. Pendergraft, "Design and Testing of a Blended Wing Body with Boundary Layer Ingestion Nacelles at High Reynolds Numbers," *43rd AIAA Aerospace Sciences Meeting and Exhibit*, Jan. 2005.

[3] D. Crichton, May 2006, personnal communication.

[4] N. A. Cumpsty, *Compressor Aerodynamics*, 1st ed. Harlow, UK: Longman scientific and technical, 1989.

[5] ——, *Jet Propulsion*, 1st ed., ser. Cambridge Engine Technology Series: 2. Cambridge, UK: Cambridge University Press, 1997.

[6] N. A. Cumpsty and J. Horlock, "Averaging Non-Uniform Flow for a Purpose," in *Proceedings of GT2005, ASME Turbo Expo 2005: Power for Land, Sea and Air*, June 2005.

[7] E. de la Rosa Blanco, "Engine design for SAX-20, Granta-3201," Jan. 2006, SAI internal document.

[8] J. D. Denton, "Loss Mechanisms in Turbomachines," *ASME Journal of Turbomachinery*, vol. 115, pp. 621 – 656, 1993.

[9] W. M. Douglass, "Propulsive Efficiency with Boundary Layer Ingestion," McDonnell Douglas, Tech. Rep. MDC J0860, Aug. 1970.

[10] A. Dowling and T. Hynes, "Towards a Silent Aircraft," Royal Aeronautical Society - Wilbur and Orville Wright Lecture, Dec. 2004.

[11] M. Drela, "Two-dimensional transonic aerodynamic design and analysis using the Euler equations," PhD Dissertation, Massachusetts Institute of Technology, Dept. of Aeronautics and Astronautics, Dec. 1985.

[12] ——, "Aerodynamics of Heat Exchangers for High-Altitude Aircraft," *Journal of Aircraft*, vol. 33, no. 1, pp. 176–184, Mar.-Apr. 1996.

[13] ——, "Aerodynamics of Viscous Fluids, MIT course 16.13," MIT Open Course Ware, <http://ocw.mit.edu/OcwWeb/Aeronautics-and-Astronautics/16-13Fall2003/CourseHome/index.htm>, Sept.-Dec. 2003.

[14] ——, "Thrust Requirement in Presence of Boundary Layer Ingestion," Oct. 2004, SAI internal document.

[15] ——, Aug. 2005, personnal communication.

[16] ——, May 2006, personnal communication.

[17] P. N. Freuler, "Boundary layer ingesting inlet design for a silent aircraft," Master's thesis, Massachusetts Institute of Technology, Dept. of Aeronautics and Astronautics, Jan. 2005.

[18] Y. Gong, "Computational Model for Rotating Stall and Inlet Distortions in Multistage Compressors," PhD Dissertation, Massachusetts Institute of Technology, Dept. of Aeronautics and Astronautics, Feb. 1999.

[19] E. M. Greitzer, "Inlet distortion in axial compressors," 1986, unpublished notes.

[20] E. M. Greitzer, C. S. Tan, and M. B. Graf, *Internal Flow, Concepts and Applications.* Cambridge, UK: Cambridge University Press, 2004.

[21] P. G. Hill and C. R. Peterson, *Mechanics and thermodynamics of propulsion.* Reading, Massachusetts: Addison-Wesley, 1992.

[22] J. H. Horlock, *Axial Flow Compressors.* London: Butterworth, 1958.

[23] I. H. Hunter and N. A. Cumpsty, "Casing Wall Boundary-Layer Development Through an Isolated Compressor Rotor," *Journal of Engineering for Power*, vol. 104, pp. 805 – 818, Oct. 1982.

[24] J. P. Johnston, "Boundary Layers in Internal Flow - Performance Prediction," in *Advanced Topics in Turbomachinery Technology*, D. Japikse, Ed. Wilder, VT: Concepts ETI, Mar. 1986, no. 2, ch. 7.

[25] D. Küchemann and J. Weber, *Aerodynamics of propulsion.* New York: McGraw-Hill, 1953.

[26] R. H. Liebeck, "Design of the Blended Wing Body Subsonic Transport," *Journal of Aircraft*, vol. 41, no. 1, pp. 10–25, Jan.-Feb. 2004.

[27] S. Lieblein, "Experimental Flow in Two-Dimensional Cascades," in *Aerodynamic Design of Axial-Flow Compressors.* NASA SP-36, 1965, pp. 183–226.

[28] J. P. Longley and E. M. Greitzer, "Inlet Distortion Effects in Aircraft Propulsion System Integration," in *Lecture Series 183*, ser. Steady and Transient Performance Prediction of Gas Turbine Engines. AGARD, May 1992, pp. 6–1–6–18.

[29] F. T. Lynch, "A Theoretical Investigation of the Effect of Ingesting Airframe Boundary Layer Air on Turbofan Engine Fuel Consumption," Douglas Aircraft Company, Tech. Rep. SM-23981, May 1960.

[30] V. Madani, "Design of a Boundary Layer Ingesting Offset Inlet for a Propulsion-Airframe Integrated Silent Aircraft," PhD dissertation, University of Cambridge, Dept. of Engineering, Apr. 2007.

[31] D. L. Rodriguez, "A multidisciplinary optimization method for designing boundary layer ingesting inlets," PhD Dissertation, Stanford University, Dept. of Aeronautics and Astronautics, 2001.

[32] M. A. Sargent, "Integration of a Boundary Layer Ingesting Inlet/Engine into a civil aircraft," University of Cambridge, Dept. of Engineering, First Year Report, Aug. 2005.

[33] ——, Feb. 2006, personnal communication.

[34] H. Schlichting, *Boundary Layer Theory.* McGraw-Hill Book Co., 1955.

[35] A. M. O. Smith and H. E. Roberts, "The Jet Airplane Utilizing Boundary Layer Air for Propulsion," *Journal of the Aeronautical Sciences*, vol. 14, no. 2, pp. 97–109, Feb. 1947.

[36] L. H. Smith, "Wake ingestion Propulsion Benefit," *Journal of Propulsion and Power*, vol. 9, no. 1, pp. 74–82, Jan.-Feb. 1993.